DR. MARTIN SARTER (Orcid ID : 0000-0003-0441-9936)

DR. MICHAL ZOCHOWSKI (Orcid ID : 0000-0002-1722-986X)

DR. VICTORIA BOOTH (Orcid ID : 0000-0003-2586-8001)

Phasic cholinergic signaling promotes emergence of local gamma rhythms in excitatory-inhibitory networks

YiqingLu[1], Martin Sarter[2], Michal Zochowski[3], Victoria Booth[4]

[1]Applied and Interdisciplinary Mathematics, University of Michigan, Ann Arbor, MI, United States

[2]Department of Psychology and Neuroscience Program, University of Michigan, Ann Arbor, MI, United States

[3]Department of Physics and Biophysics, University of Michigan, Ann Arbor, MI, United States

[4]Departments of Mathematics and Anesthesiology, University of Michigan, Ann Arbor, MI, United States

Corresponding authors:

Victoria Booth, vbooth@umich.edu and Michal Zochowski, michalz@umich.edu

Abbreviated title: Phasic ACh promotes emergence of local gamma rhythms

Data Accessibility: All computer codes implementing model results will be posted on a publicly accessible site upon publication of the manuscript.

Author Contributions:V.B. and M.Z. conceived the model, designed the study and analyzed results. Y.L. implemented the model, performed the numerical simulations and analyzed results. M.S. provided critical feedback that shaped the study. All authors discussed results and contributed to writing the final manuscript.

Word count: 6,241

Figure count: 7

List of Abbreviations

ACh	acetylcholine
E	excitatory
I	inhibitory
PING	Pyramidal-Interneuronal Network Gamma
g_{Ks}	Maximalconductance of M-type K+ membranę ioniccurrent
BF	Basalforebrain
mAChR	Muscarinic M1 acetylcholine receptor
nAChR	Nicotinicacetylcholine receptor
LFP	Local field potential
I-f	Input-frequency
PRC	Phaseresponsecurve

ING	Interneuron Network Gamma

Abstract

Recent experimental results have shown that the detection of cues in behavioral attention tasks relies on transient increases of acetylcholine (ACh) release in frontal cortex and cholinergically-driven oscillatory activity in the gamma frequency band(Howe *et al.*, 2017).The cue-induced gamma rhythmic activity requires stimulation of M1 muscarinic receptors.Usingbiophysical computational modeling, we show that a network of excitatory (E) and inhibitory (I) neurons, that initially displays asynchronous firing, can generate transient gamma oscillatory activity in response to simulated brief pulses of ACh. ACh effects are simulated astransient modulation of the conductance of an M-type K^+ current which is blocked by activation of muscarinic receptors and has significant effects on neuronal excitability. TheACh-induced effects on the M-current conductance, g_{Ks}, change network dynamics to promote the emergence of network gamma rhythmicity through a PING mechanism. Depending on connectivity strengths between and among E and I cells, gamma activity decays with the simulated g_{Ks}transient modulation or is sustained in the network after the g_{Ks}transient has completely dissipated. We investigated the sensitivity of the emergent gamma activity to synaptic strengths, external noise and simulated levels of g_{Ks} modulation. To address recent experimental findings that cholinergic signaling is likely spatially focused and dynamic, we show that localized g_{Ks} modulation can induce transient changes of cellular excitability in local subnetworks, subsequently causing population-specific gamma oscillations. These results highlight dynamical mechanisms underlying localization of ACh-driven attentional responses and the emergence of dominance of ACh-driven cell populationswithin a network.

Significance Statement

Neuromodulation of cortical regions by acetylcholine has traditionally been assumed to be temporally slow and spatially diffuse. Recent experiments, however, indicate that cholinergic signaling is fast and spatially localized in the context of attentional performance tasks. Additionally, cholinergic transients generated gamma frequency oscillations that contributed to

successful attentional performance. Using computational modeling, we show that transient cholinergic modulation of neural excitability induced the emergence of transient synchronous gamma activity from a background of asynchronous firing in excitatory-inhibitory neural networks. Spatially localized simulated cholinergic modulation generated spatially localized gamma rhythms. Given the importance of gamma rhythms in cognitive processing, these results suggest that spatially localized, cholinergically-induced gamma may contribute to selectivity in the processing of competing external stimuli, as occurs in attentional tasks.

Introduction

Cholinergic neurons situated in the basal forebrain (BF) project to virtually all cortical layers and regions. In contrast to traditional descriptions of this projection system as "diffusely organized" and involved in the relatively slow regulation of cortical activity states, contemporary evidence indicates the presence of BF subpopulations of neurons with highly topographically organized afferent and efferent projections (Zaborszky *et al.*, 2005; Zaborszky *et al.*, 2015; Gielow & Zaborszky, 2017; Yuan *et al.*, 2018) and, in cortex, of spatially and temporally discrete, fast, phasic or "transient" cholinergic signaling (Parikh *et al.*, 2007). Because cortical cholinergic activity is necessary for attentional performance in rodents and humans (McGaughy *et al.*, 1996; Kim *et al.*, 2017), the role of cholinergic transients has been investigated specifically in the context of attentional performance. In rats performing a signal detection-based attention task, cholinergic transients were found to be evoked by cues that were successfully detected, but not by missed cues (Howe *et al.*, 2013). Moreover, optogenetic suppression and generation of transients indicated that cholinergic transients are necessary and sufficient for the detection of cues in such contexts (Gritton *et al.*, 2016). Transient cholinergic signaling has been proposed to account for a range of behavioral and cognitive functions which traditionally have been associated with more slowly (over minutes) changing extracellular ACh levels (Sarter & Lustig, 2019).

Consistent with the finding that cholinergic transients are necessary to force a relatively complex behavioral response, the determination of their postsynaptic impact indicated that these transients generate high-frequency oscillations in the gamma range in frontal cortex, and that gamma oscillations remain active through the cue-response period. Moreover, generation of gamma oscillations requires local, frontal stimulation of muscarinic M1 ACh receptors

(mAChRs). Blocking M1-mediated increases in gamma power was sufficient to reduce cue detection rates (Howe *et al.*, 2017). The present study was guided by questions about the potential, neuronal network-based mechanisms which allow brief, phasic ACh release events to generate such impactful high-frequency oscillations.

Using biophysical models of networks of excitatory and inhibitory neurons we show that simulated transient ACh modulation throughmAChRs can induce network gamma rhythmicity. As previously shown (Borgers *et al.*, 2005);(Tiesinga *et al.*, 2001), simulated mAChR effects on membrane potassium currents can promote tonic synchronous network oscillatory activity in the gamma band through a PING mechanism. While these previous results suggest that transient ACh modulation should be able to result in transient gamma band oscillatory activity, many questions remain regarding network and modulation conditions that support reliable generation and dissolution of transient gamma rhythmic activity. In this study, we particularly focus on the characteristics of transient ACh modulation and network properties that allow the transient emergence of gamma oscillations from background asynchronous, non-rhythmic activity. The role of acetylcholine in attentional modulation of neural network responses has been previously investigated in computational models of diverse brain networks (Hasselmo *et al.*, 1992; Tiesinga *et al.*, 2001; Borgers *et al.*, 2005; Borgers & Kopell, 2008; Deco & Thiele, 2011) (see (Newman *et al.*, 2012)and (Thiele & Bellgrove, 2018)for reviews). Here, we concentrate onACh-induced effects on neuronal excitability that generate transient gamma band rhythmicity that is associated with attentional performance. We show that spatially-localized transient ACh modulation can induce spatially-localized transient gamma oscillations which can act as a substrate for attentional selectivity in network processing of external stimuli. However, we also show, that the parametric region in which gamma oscillationsare readily generated due to ACh increase is bistable. This means that reduction of ACh tone alone may not lead to its abolition – noise or other desynchronizing agentsare needed for prompt gamma dissolution.

Methods

Neuron model

All neurons in the network are modeled using a Hodgkin-Huxley-type model that includes a Na^+ current, a delayed rectifier $K+$ current and a leak current. An additional M-type slow $K+$ current is added to simulate modulation by acetylcholine via mAChRs(McCormick & Prince, 1985;

Krnjevic, 2004; Stiefel *et al.*, 2009). The maximum conductance g_{Ks} of the M-type K+ current is the parameter that represents the amount of ACh modulation. In general, g_{Ks} is set between 0 mS/cm² and 1.5 mS/cm² with low g_{Ks} corresponding to large concentration of ACh. The current balance equation for each neuron is

$$C\frac{dV}{dt} = -g_{Na}m_\infty^3 h(V - E_{Na}) - g_{Kd}n^4(V - E_K) - g_{Ks}z(V - E_K) - g_L(V - E_L) + I_{app} + I_{noise} - I_{syn}$$

where $C = 1\mu F$/cm². V represents the membrane voltage in millivolts and t is time in milliseconds. g_{Na}, g_{Kd}, g_{Ks} and g_L are maximal conductances of the corresponding currents. In all the cells, $g_{Na} = 24$ mS/cm², $g_{Kd} = 3$ mS/cm², $g_L = 0.02$ mS/cm². g_{Ks} is varied as described below. To show the influence of g_{Ks} on neuronal excitability, the neuronal input-frequency curve is plotted for various values of g_{Ks} (Figure 1C). The E_{Na}, E_K, E_L are the reversal potentials for sodium, potassium and leak currents, where $E_{Na} = 55$mV, $E_K = -90$mV, $E_L = -60$mV, respectively. I_{app} represents the externally applied current to both excitatory and inhibitory cells. I_{syn} models the synaptic input current that the cell receives from all other connected cells in the network (see below). I_{noise} represents external Poisson noise delivered to each cell (see below). The m_∞, h, n, z are unitless gating variables of the corresponding current activation, with their evolution given by general equation:

$$\frac{dX}{dt} = \frac{X_\infty(V) - X}{\tau_X(V)} \text{for} X = h,n,z$$

where

$$m_\infty(V) = \frac{1}{1 + e^{(-V-30)/9.5}}$$

$$h_\infty(V) = \frac{1}{1 + e^{(V+53)/7.0}}$$

$$n_\infty(V) = \frac{1}{1 + e^{(-V-30)/10}}$$

$$z_\infty(V) = \frac{1}{1 + e^{(-V-39)/5}}$$

$$\tau_h(V) = 0.37 + \frac{2.78}{1 + e^{(V+40.5)/6}}$$

$$\tau_n(V) = 0.37 + \frac{1.85}{1 + e^{(V + 27)/15}}$$

$$\tau_z(V) = 75$$

Heterogeneity in cell dynamics is introduced by varying the external driving current I_{app} to every excitatory cell (I_{app} is different for every cell but kept constant throughout the simulation). The amplitude of this external current is chosen to make the intrinsic firing rates of excitatory cells for baseline g_{Ks} (0.6 mS/cm^2) follow a normal distribution with mean frequency of 50 Hz and standard deviation of 5 Hz. Thus, based on the neuronal input-frequency curve (Figure 1C), I_{app} values were chosen between 2.814 µA/cm^2 and 3.427 µA/cm^2. For every inhibitory cell, the baseline current is chosen from a uniform distribution, with mean near current threshold (-0.2 µA/cm^2) and standard deviation 0.02 µA/cm^2.

Network structure

The E-I network consists of 1000 neurons, among which 800 neurons are excitatory and 200 neurons are inhibitory. The connectivity between every pair of neurons is randomly assigned. Each E cell receives pre-synaptic input from other E cells with probability of 5% (unless otherwise specified) and from inhibitory cells with probability of 30%. Each I cell receives pre-synaptic input from all other cells (both excitatory and inhibitory cells) with probability 30%. This connectivity is based grossly on that experimentally reported (Ascoli & Atkeson, 2005; Viriyopase *et al.*, 2016).

In the simulations shown in Figure 7, the excitatory cells are divided randomly into two groups with 400 neurons in each group. Other connectivity probabilities are kept the same except that the probability that two excitatory cells from different groups are connected is reduced to 0.5%.

The synaptic current is modeled with a double-exponential profile:

$$I_{syn}(t) = w_{syn}(V - E_{syn})(\sum_{s_i} e^{-(t - s_i)/\tau_d} - e^{-(t - s_i)/\tau_r})$$

In the equation, τ_d is the decay time constant and τ_r is the rise time constant. In the simulations, $\tau_d = 3$ ms for excitatory synapses, $\tau_d = 5.5$ ms for inhibitory synapses, $\tau_r = 0.2$ ms for all the synapses. The s_i are the firing times of the spikes of presynaptic neurons. V is the membrane

voltage of post-synaptic neuron and E_{syn} is the reversal potential of the synaptic current, which is set to be 0 mV for excitatory synapses and -75 mV for inhibitory synapses; w_{syn} is the maximal conductance of the synaptic current or synaptic strength. The default values are w_{ee}=0.004 mS/cm^2, w_{ii}=0.016 mS/cm^2, w_{ei}=0.002 mS/cm^2, w_{ie}=0.003 mS/cm^2. In Figure 3 and Figure 6, synaptic conductances were varied as indicated.

Transient ACh pulse

ACh modulation was modeled as a brief reduction in the maximal conductance of the M-current, g_{Ks}, simulating the post-synaptic effect of AChmediated by mAChRs. The baseline g_{Ks} value, $\overline{g_{Ks}}$, in the excitatory cells and inhibitory cells was set to be 0.6 mS/cm^2 and 0 mS/cm^2, respectively (except for simulations in Figure 4 and Figure 6 c, d, e, f). The g_{Ks} transient was modeled by $\overline{g_{Ks}} - \Delta g_{Ks}(t)$, where $-\Delta g_{Ks}(t)$ is a piecewise function with an initial linear decrease and an exponential recovery (see Figure 2a):

$$\Delta g_{Ks}(t) = \begin{cases} 0 & if\ t \leq t_p \\ \Delta g_{Ks} \cdot \dfrac{t - t_p}{t_d} & if\ t_p < t \leq t_p + t_d \\ \Delta g_{Ks} \cdot e^{-\frac{t - t_p - t_d}{c_r}} & if\ t > t_p + t_d \end{cases}$$

where t_p is the time that the transient starts and was set to 2000 ms in all simulations. The decay time t_d was set to 100 ms, so the maximum g_{Ks} reduction occurred at 2100 ms. c_r is the recovery constant which reflects the time of g_{Ks} recovery and was set to c_r=3600 ms. With this value, g_{Ks} recovers to very close to $\overline{g_{Ks}}$ after approximately 1500 ms. Δg_{Ks} represents the amplitude of the g_{Ks} transient and its default setting is 0.6 mS/cm^2 (except in Figure 4). In Figures 2-5 and 7, the g_{Ks} transient is applied only to excitatory cells. In Figure 4, $\overline{g_{Ks}}$ and Δg_{Ks} are varied to study their influence on emergent gamma oscillations. In Figure 6 c,d, the default g_{Ks} transient is applied to only inhibitory cells, and in Figure 6 e,f, it is applied to all cells.

Poisson Noise

In Figures 2, 5 and 7, in addition to heterogeneity introduced by different external driving current I_{app}, random external noisy input in the form of Poisson distributed, brief, depolarizing 'kick'

stimuli were applied to both the excitatory cells and inhibitory cells to simulate background noise outside the network from other parts of the brain. In each simulation, the amplitude and Poisson rate of kicks to all cells are fixed at same values. Each kick was a square applied current pulse of duration 1 ms.

Simulation

The codes implementing the simulations were written in Matlab. All simulations were run for 4000 ms. Initial conditions for membrane voltages and gating variables were set randomly. Initial conditions for V ranged between -62 mV to -22 mV; initial conditions for n, h, and z ranged between 0.2 and 0.8, 0.2 and 0.8, and 0.15 and 0.25, respectively. The ordinary differential equation system is solved by fourth order Runge-Kutta method. Results shown in Figures 3-6 were averaged over 5 simulations.

In sample raster plots in Figures 2, 3 and 7, red represents excitatory cells with indices from 1 to 800 (red and green in Figure 7) and blue represents inhibitory cells with indices from 801 to 1000. The excitatory cells are sorted so that the cells with the highest driving current I_{app} are assigned the lowest index, while the cells with lowest driving current are assigned the highest index. The two groups of excitatory cells are sorted separately in Figure 7.

Measures

Synchrony measure is used to quantify how well the cells are synchronized in the network by measuring the degree of spike coincidence (Golomb & Rinzel, 1993; 1994). Spike trains for each cell are first convolved with a Gaussian function to form a simulated spike trace, $V_i(t)$. The Gaussian is in the form $g(t) = e^{-\frac{(t-t_0)^2}{1.6}}$ where t_0 is the spike time. The averaged spike trace over all cells V(t) is defined as $V(t) = \frac{1}{N}\sum_{i=1}^{N}V_i(t)$ where N is number of the cells. The variance of individual spike traces σ_i and the variance of the average spike trace σ are defined as

$$\sigma_i = \ < V_i(t)^2 > - \ < V_i(t) >^2$$
$$\sigma = \ < V(t)^2 > - \ < V(t) >^2$$

where $<>$ is the time average over the interval during which synchrony is measured. The synchrony measure is defined as

$$S = \frac{\sigma}{\frac{1}{N}\Sigma_{i=1}^{N}\sigma_i(t)}$$

Therefore, S=0 indicates complete asynchrony and S=1 indicates complete synchrony.

In the figures, synchrony measures are calculated in different intervals relative to the simulated ACh pulse. As the major part of the pulse is contained in the time interval from 2050 ms to 2550 ms, synchrony measure is calculated over this interval to describe network activity during the pulse. Spikes from 1500 ms to 2000 ms and spikes from 3500 ms to 4000 ms are used to calculate the synchrony measure before the pulse and after the pulse, respectively.

To determine duration of synchrony in Figure 5, the synchrony measure of inhibitory cells from 2000 ms to 4000 ms was calculated in 20 time windows of length 100 ms. Time windows with synchrony measure greater than 0.7 were considered synchronized. The threshold of S = 0.7 for inhibitory cells was chosen from observations of raster plots.

The Fourier transform was used to compute the change of power in each frequency band over time. To compute the power spectrogram, simulated spike traces, obtained by convolving spike trains of each cell with the Gaussian function above, were summed across all excitatory cells to simulate a local field potential (LFP). The Fourier transform was applied to the simulated LFP in sliding time windows to obtain the power spectrum over time. The window width was 500 ms with a sliding step size of 10 ms.

In Figure 7, average firing frequency is calculated in a sliding time window to show frequency changes over time. To compute, we define N_k as the number of times that cell k fires in a time window of length T = 500 ms and then compute the average firing frequency in the time window as

$$f = \frac{\Sigma_{k=1}^{j}N_k}{jT}$$

The summation is over the groups of ACh modulated and non-ACh modulated excitatory cells and inhibitory cells separately where j is the number of cells in each group. Average firing frequency in computed in each 500 ms time window with a 10 ms sliding step size.

Results

ACh modulation ofneural response properties

Acetylcholine (ACh) modulatesintrinsicmembrane excitabilityof a neuron through muscarinic and nicotinic receptors (m/nAChRs). Guided by neurophysiological evidence, here we concentrated on the effects of ACh modulation through mAChRs and theiraction on the slow, hyperpolarizing voltage-gatedK^+M-current. We modeledneuronal dynamics using a biophysical cell model based on the Hodgkin-Huxley formalism that incorporates the M-current in addition to spike-generating Na^+ and K^+ ionic currents. The model,originally developed by Stiefel et al.(Stiefel *et al.*, 2009),is based on experimental recordingsof ACh modulation ofvisual cortex principal cells(Stiefel *et al.*, 2008)(see Methods for details). We varied the maximal conductance (g_{Ks}) of the M-current in excitatory cells as a proxy for the local ACh level, with g_{Ks}=0 mS/cm^{2}corresponding to high ACh level (down-regulation of the M-current) and g_{Ks}=1.5 mS/cm^2 corresponding to lowest AChlevel (up-regulation of the M-current). Here, we specifically investigated the emergence of transient gamma band rhythmic network activity due to transient increase of ACh level, simulated by transient decrease in g_{Ks}, mimicking phasic ACh release measured during cued response attentional tasks (Howe *et al.*, 2017).

In this neural model, changes in g_{Ks}conductance valuesresult in changes to the neuronal input-frequency (I-f) dependence. Namely, with decreasingg_{Ks}, the neuronal input-frequency (I-f) curve changes froma discontinuous profile (Type II) to a continuous profile (Type I) (Figure 1c) and, at the same time, the neural membrane becomes significantly more excitable, with lower g_{Ks} significantly elevating the frequency response of the cell to the same level of input. Additionally, decreasing g_{Ks} induces a simultaneous change in the neuronal phase response curve (PRC) (Figure 1d) (Stiefel *et al.*, 2008). The PRC profile changes from Type II for which either delays or advances in spike timing can be induced by a brief excitatory stimulus depending on its timing, to Type I for which spike timing is only advanced by the stimulus. Previous analytical and numerical work has shown that neurons with Type II PRCs are more prone to synchronize compared to cells with Type I PRCs (Ermentrout, 1996; Bogaard *et al.*, 2009; Fink *et al.*, 2011).We initially focused on g_{Ks} modulation of excitatory cell responses(g_{Ks}set to 0 mS/cm^2 in inhibitory cells), but also considered g_{Ks} modulation of both cell types.

Model networkswere composed of 800 excitatory (E) and 200 inhibitory (I) neurons with random connectivityamong and between each cell type(Figure 1a, see Methods for details).Cells additionally received noisy external synaptic input. First, we investigatedeffects of global transient g_{Ks} modulation on the generation of transient gamma rhythmic synchronous dynamics in the network, then we consideredspatially localized, transientg_{Ks} modulation in a network consisting of two subpopulations of E cellswhere only onewas modulated(Figure 1b), and investigatedspatially localized generation of transient gamma oscillatory dynamics.

Phasic ACh release promotes emergent gamma oscillations

In our E-I network model,transient decrease of g_{Ks}changedthe network dynamical regime from asynchronous activity to gamma band oscillations. Interestingly, the emergent gamma could be maintained as a stable state in the network after the phasic g_{Ks} hadrecovered, or could be destabilized through external noise, causing the network to revert back to the asynchronous state when the g_{Ks} transient dissipated. Figure 2 depicts an example oftransient emergent gamma in response to phasic g_{Ks} modulation. Here, the E cells wereassumed to contain muscarinic receptors that induce a transient decrease in g_{Ks} (Figure 2a).

To detect emergence of rhythmic network activity, we computed the Fourier transform of the simulated local field potential (LFP, see Methods)to show characteristics of network activity inthe frequency domain (Figure 2b). Initially, cells fired asynchronously with no rhythmic activity apparent across the network. Keeping all other network parameters the same, as g_{Ks} decreased, firing rates of all the cells in the network rapidly increased due to changes in E cell intrinsic excitability (Figure 1c). During the g_{Ks} decrease, increased power at very low frequencies was observed due to the sharp rise in overall network activity and the simulated LFP.The increased activity from excitatory cells led to the emergence of gamma frequency band synchrony through the so-called Pyramidal Interneuron Gamma (PING) process(Whittington *et al.*, 2000; Borgers & Kopell, 2005)(Tiesinga & Sejnowski, 2009). In this process, the increased excitation from E cells leads to increased firing and synchronization of I cells. This, in turn, leads to silencing of the E cells, which when released from inhibition fire synchronously, subsequently driving another synchronous burst of inhibition. Here, gamma band synchrony emerged as I cell synchrony consolidated during the decrease in g_{Ks}(Figure 2c) and gamma decayed as g_{Ks}

recovered (Figure 2d). Below, we analyze the reliability of the emergence and maintenance of this gamma band synchrony as important properties are varied, such as synaptic strengths, the presence of external noise and the efficacy of simulated ACh on the M current. This analysis reveals that inducing gamma rhythms transiently from a background of asynchronous activity depends sensitively on network and modulation characteristics.

Sensitivity of emergent gamma to network connectivity

We next investigated to what extent emergence of ACh mediated gamma band oscillations depended on the properties of network connectivity. To isolate network connectivity effects,the external noisy inputto cells was not included. We varied the magnitude of the synaptic conductancesfrom I to E cells (I-E synapses, w_{ie}y-axis, Figure 3 a-c) and within the excitatory (E-E connectivity, w_{ee}) and inhibitory (I-I connectivity, w_{ii}) subnetworks (x-axis, Figure 3 a-c) keeping E-I synaptic strength fixed(w_{ei} fixed at 0.002 mS/cm^2).The resultant network dynamics, quantified by the synchrony measure (color in Figure 3 a-c, see Methods), within thisconnectivity parameter space could be divided roughly into three regimes(Figure 3d, e, f).

With low I-E connectivity, the E-I networkdid notfully synchronize in response to the g_{Ks} transient (Figure 3d, bottom region, w_{ie}<0.002 mS/cm^2). Although excitability of the excitatory cells rose during the g_{Ks} decrease and therefore inhibitory cells received more input from excitatory cells and became more synchronized, the low I-E synaptic conductance, however, stopped the inhibitory cells from synchronizing the excitatory cells to form PING rhythmicity across the network. Thus, the excitatory cells fire asynchronouslybefore, during and after the g_{Ks} pulse.

For moderate values of I-E connectivity (w_{ie} between 0.002 - 0.005 mS/cm^2),the network firedasynchronously before the g_{Ks} transient and synchronized to form gamma oscillations during the transient (Figure 3e). Synaptic strength values for the results shown in Figure 2 are in this regime. Interestingly, for some synaptic strength values within this parameter range,gamma synchrony could be maintainedeven after the g_{Ks} transient ended (Figure 3e, right panel), indicating that the network stably generatesboth asynchronous firing and gamma rhythmicity, and that the g_{Ks} pulse switches the network between these two regimes. Experimentally,ACh-induced gamma band synchrony has been observed only transiently, indicating lack of stability

of the synchronous gamma regime.We show below that maintained gamma synchrony after dissipation of theg_{Ks} transient can be easily destabilized byexternal noisy input to the network.

Finally, for high I-E connectivity (w_{ie}>0.005 mS/cm²), the network remains synchronized before,during and after the g_{Ks} transient, with increased E cell excitability during the pulse acting to increase the frequency of synchronous firing (Figure 3f).

We note that in the low w_{ie} regime, the I cells were generally more synchronized than the E cells. This I cell synchrony is similar to interneuron network gamma (ING) synchrony since it is generated by the recurrent synaptic coupling among the I cells (Whittington *et al.*, 2000; Tiesinga & Sejnowski, 2009). In some definitions of ING, the I cells should be intrinsically spiking; here not all I cells spike without input, but the mean external driving current to I cells is close to their current firing threshold and excitation from the E cells promotes their firing. With this characterization of low w_{ie} regime dynamics, the moderate w_{ie} regime exhibits bistability between ING and PING dynamics where either state is observed, and the high w_{ie} regime displays only PING dynamics. In separate simulations, we explicitly tested bistability of ING and PING solutions in the moderate w_{ie} regime and verified that either solution is maintained depending on the initial conditions of the network state (results not shown).

These results show that inducing transient gamma rhythmicity requires network connectivity characteristics near the regime supporting both ING andPING synchrony. This may restrict properties of the asynchronous network states from which transient ACh can generate gamma oscillations.

Sensitivity of emergent gamma to simulated ACh level

We next investigated how the magnitude of simulated effects of ACh on the maximal conductance of the M-current, g_{Ks}, affected the emergence of gamma rhythmicity (Figure 4). To model theg_{Ks}pulse,$g_{Ks}$was set initially to a baseline value,$\overline{g_{Ks}}$, representing the absence or a low ACh level. During the pulse, $g_{Ks}$was dropped to$\overline{g_{Ks}}-\Delta g_{Ks}$as the ACh transient reached its peak. Thus, we can relate $\Delta g_{Ks}$to the peak magnitude of the post-synaptic effects of the ACh pulse. Afterwards, g_{Ks}recovered exponentially back to the baseline level, following the time course depicted in Figure 2a. To measure the efficacy of the g_{Ks}pulse to induce gamma, we measure network synchrony before the pulse (when $g_{Ks} = \overline{g_{Ks}}$, Figure 4a), during the g_{Ks}transient (Figure

4b), and subsequently calculate the difference (Figure 4c) for E cells (Figure 4, top panels) and I cells (Figure 4, bottom panels) separately.

Results in the parameter space spanned by $\overline{g_{Ks}}$(y-axis) and Δg_{Ks}(x-axis) could be divided into three regimes based on observed dynamics of the network (only values above the diagonal were considered to ensure that the lowest g_{Ks} value during the pulse, $\overline{g_{Ks}} - \Delta g_{Ks}$, was not negative). In the lower left corner, baseline $\overline{g_{Ks}}$is low, and$\Delta g_{Ks}$is small amplitude (due to the g_{Ks} range constraints). Here, even beforethe g_{Ks}pulse was applied, the excitatory cells displayed high excitability driving emergence ofPING synchrony.During the ACh pulse, the dynamics didn't change significantly, resulting in a differencein synchrony near zero (Figure 4c).

In the intermediate baseline regime (for$\overline{g_{Ks}}$ between 0.4 and 0.8 mS/cm^2), the network exhibited asynchronous dynamics before the g_{Ks}pulse. The left hand side of this regime corresponds to low magnitude of ACheffects (Δg_{Ks} small). Here, the increase of excitability of the excitatory cells associated with the g_{Ks}pulsewas not sufficient to drive PING synchrony, and the network remained in an asynchronous firing regime during the g_{Ks} pulse. However, for larger Δg_{Ks}values (center right part of this regime), increased E cell excitability mediated the formation of gamma synchrony during the g_{Ks} pulse (Figure 4b). This results in a significant increase in synchrony difference (Figure 4c).

In the third regime for highbaseline g_{Ks}($\overline{g_{Ks}}$ > 0.8), the network exhibited strong synchrony before theg_{Ks} pulse. This synchrony was, however, not solelymediated by the PING mechanism, as the E cell excitability that drives PING was significantly decreased in this regime.Instead, synchrony was additionallysupported by changes in neuronal response properties obtained with high g_{Ks} values, specifically changes in the PRC. As shown in Figure 1d, for large g_{Ks} values,the profile of the phase response curve changes from Type I to Type II facilitating promotion of synchrony. Separate simulations of the network in this regime verify that when synaptic connections from the I cell to the E cells were blocked (w_{ie}= 0mS/cm^2) synchrony was observed although the synchrony measure was higher with I to E synapses intact due to the PING mechanism (results not shown). Here, in this parameter regime, large Δg_{Ks}decreasedM-current conductance and subsequentlyshiftedthe PRC toward a Type I profile resulting in weakened synchrony. Hence, within this regime, the effect of the g_{Ks} pulse is essentially reversed with less synchrony being observed during the pulse as compared to before its presentation.

Thus, the emergence of transient gamma rhythmicity from a background of asynchronous activity requires sufficient magnitude of the mAChR mediated post-synaptic effects and tight control of those effects in the absence of ACh.

Effects of external noise on duration of emergent gamma

Next, we investigated how external noise affects stability of the emerging synchronous gamma oscillations during the g_{Ks} transient. This was particularly important as we observed that for noiseless network simulations gamma oscillations could be maintained after the g_{Ks} transient subsided. Such a stability in gamma band oscillations is not observed experimentally. Here, external noise was simulated by brief,depolarizing 'kick' stimuli arriving to E and Icells at random times, governed by a Poisson process (see Methods). We measured the duration of synchronous gamma oscillations after the onset of the g_{Ks} transient as a function of the amplitude and average frequency of the kickstimuli (Figure 5).As expected, stronger and/ormore frequent kickstimuliled to shorter duration of synchronous gamma (Figure 5).When both the rate and amplitude of the noisy kickswere small (Figure 5; bottom left corner), synchronous gamma oscillations remained stable indefinitely after theg_{Ks} transient. On the other hand, when rate and amplitude were both large (Figure 5; top right corner), the network didn't achieve a synchronized state even at the minimum of the g_{Ks} pulse. In the intermediate regime, as the rate and amplitude of kicks increased, the time duration of the synchronous state decreased; moreover, we found that, in this regime, the duration of gamma oscillationsrarely exceeded the duration of the g_{Ks} pulse. In summary, excessive noisy conditions in the network inhibits the emergence of gamma rhythmicity and its duration.

Only AChmodulation of excitatory cells promotesstrong emergent gamma

In the simulations reported above,simulated ACheffects on the M-current occurred only in the E cells. However, it is known that there are inhibitory interneuron types that have muscarinic receptors(Disney & Aoki, 2008). Thus, we investigated whether incorporating ACh modulation of the M-current in I cells,instead of E cells, or in both E and Icellscould produce synchronous gamma oscillations(Figure 6).The figure displays thedifferences in network synchrony measured in the E cells (top panels) and in the I cells (bottom panels) between beforeand during the g_{Ks} transient (left panels), and between before and after the g_{Ks} transient (right panels). As the

network connectivity regimes where gamma synchrony can occur in these cases may vary, we considered the full ranges of network synaptic strengths where E cell g_{Ks} modulation had the strongest effects (as in Figure 3; for example, Figure 6a displays the difference of Figure 3b and Figure 3a). We observed that g_{Ks} modulationof the E cells had the most pronounced effects for the transition to gamma band synchrony (Figure 6 a,b), whereas g_{Ks} modulation to only the I cells (Figure 6 c,d) or to both E and I cells (Figure 6 e,f) induced only slight changes in network synchrony.

When only I cellswere modulated (Figure 6 c, d), the g_{Ks} transient caused increases in synchrony only for network connectivity parametersin the regime where E cells showed synchronous firing prior to the g_{Ks} transient (see Figure 3a). However, for high w_{ii} values (lower right corner), synchrony of I cells dropped during the g_{Ks} pulse, due to increased excitability leading to increased inhibition among them. With almost all connectivity parameters, network dynamics returned to their initial state after the g_{Ks} pulse even without the presence of external noise.

When g_{Ks}modulation was applied to bothE and Icellssimultaneously (Figure 6 e,f), we observed increases in gamma bandsynchrony only with the combination of small I-E connectivity and relatively small intra-connectivity.But again networks returned to their initial state after the g_{Ks} transient.

Hence, emergence of gamma rhythmicity depended strongly on mAChR-mediated effects primarily occurring in excitatory cells.Simulated ACh modulation of only the I cells resulted in increases in gamma synchrony in parameter regimes exhibiting synchrony before the modulation, similar to previously reported effects of attentional modulation of I cells (Buia& 2006).

Spatially localized ACh modulation induces spatially localized gamma

Finally, since recent experimental results indicate that cholinergic signaling is spatially focused rather than broadly distributed across networks(Sarter & Lustig, 2019), we investigated effects of spatially localized g_{Ks}modulation on generation of spatially localized gamma oscillations. Here, E cells are divided into two groups (Figure 1b) – only the targeted group (red) receivedg_{Ks} modulation;in the non-targeted group (green) g_{Ks} remainedat its baseline levelthroughout the

simulation (Figure 7). As the transient was applied to the targeted excitatory group, its firing rate, as observed earlier, significantly increased (Figure 7a,d). This increased excitatory drive increasedI cell firing and eventually caused them to synchronize. All E cells, including the non-targeted group, received inhibitory signaling. As a consequence, firing frequency in the non-targeted group decreased (Figure 7a,d). As I cell synchrony consolidated, PING mediated gamma band oscillations emerged in both E cell groups (Figure7b,c,e), however power in the gamma frequency bandwas significantly stronger in the targeted group than in the non-targeted group.Gamma oscillations were weak in the non-targeted group due to theirlower excitability that caused longer recovery times from the synchronous inhibitory input. The increased excitability of the E cells in the targeted group allowed them to recover faster and generate another burst of excitation to drive the next inhibitory burst before the non-targeted E cells could fully recover. Hence, the targeted group displayed both significant enhancement of firing frequency and power of gamma band synchrony over the non-targeted group. This spatial localization of gamma band oscillationspossibly providesfor enhanced firing pattern readout from localized ensembles of cells within a network.

Discussion

Motivated by recent evidence for fast, phasic and spatially localized ACh signaling in cortical networks and its generation of transient gamma rhythmicity, we investigated its underlying neuronal network-based mechanisms using biophysical computational modeling of E-I networks. Post-synaptic ACheffects were simulated by the blockade of the muscarinic M-type K$^+$conductance g_{Ks}in excitatory cells based on experimental evidence showing the reliance on muscarinic receptors for the generation of gamma rhythmicity(Howe *et al.*, 2017). Our resultsshow that simulated ACh transients, causing increases in E cell excitability, induced gamma band rhythmic firing through a PING mechanism, as might be inferred from previous findings (Borgers *et al.*, 2005)(Tiesinga *et al.*, 2001; Buia & Tiesinga, 2006; Buia & Tiesinga, 2008; Tiesinga & Buia, 2009). However, we show that the reliability of the generation of gamma rhythmicityfrom a background of asynchronous activity depends sensitively on important network and modulation characteristics. In particular, the emergence of gamma oscillations depended on synaptic connection strengths among E cells and among I cells, while connection strengths from I to E cells had a larger role in causing synchronous gamma oscillations in the

absence of simulated ACh. The presence of external noise in the network affected the generation and duration of gamma oscillations. Interestingly, for some network connectivity regimes in the absence of external noise, induced gamma oscillations were sustained even after the simulated ACh transient completely dissipated. This suggests that networks can support bistable states involving PING dynamics, and conversely, that external mechanisms might be needed to eliminate gamma oscillation after ACh diminishes. Including simulated ACh modulation of the I cells, in addition to or instead of the E cells, was not as effective in generating gamma oscillations, although it affected synchrony as previously shown (Buia & Tiesinga, 2006). Lastly, we showed that spatially localized simulated ACh modulation induced gamma oscillations in a subset of cells in a network without recruiting the entire network in the rhythmic activity, which may contribute to the selective processing of stimuli (see below).

In the behavioral cue detection experimental results, the observed ACh induced gamma band activity occurred over a range of frequencies (Howe *et al.*, 2017). Specifically, in response to the cue, there was an initial burst of high-frequency gamma synchrony (75 - 90 Hz) followed by longer-lasting lower gamma frequency activity (47 – 57 Hz). Our simulation results show a similar variation of gamma frequency in response to the g_{Ks} pulse, namely frequencies decrease over the range of approximately 90 to 50 Hz during the pulse (see Figure 2b). This frequency decrease follows the time course of the g_{Ks} transient, however the frequency values are determined by the PING mechanism. While the experimentally observed high and low frequency gamma activity may be associated with different mechanisms (Howe *et al.*, 2017), our results suggest that a variation in gamma frequency can be the result of variation in the efficacy of ACh modulation.

In this study, we focused on the modulation of cortical circuitry mediated by muscarinic cholinergic receptors (mAChRs). In the motivating experimental study, Howe et al. (Howe *et al.*, 2017) concluded that activation of mAChRs was the basis for the long lasting gamma rhythms induced by cue-associated ACh transients. Cholinergic effects mediated by nicotinic receptors (nAChRs), on the other hand, modulated only initial transient gamma activity observed at cue onset. As additional justification, based on effects of nAChR activation in neocortical circuits (Colangelo *et al.*, 2019), their effects may also act to contribute to generation of gamma oscillations by the mechanisms described here. Specifically, activation of nAChRs pre-synaptically modulates cortical pyramidal cell synaptic transmission leading to increases in

glutamatergic synaptic signaling. Some studies report that inhibitory interneuronsare the post-synaptic targets of the boosted signaling (Couey *et al.*, 2007; Obermayer *et al.*, 2018; Urban-Ciecko *et al.*, 2018). These effects align with the PING mechanism for gamma oscillations that relies on strong excitatory drive to inhibitory cells, and with previous modeling studies showing promotion of ING and PING synchrony with increased excitatory drive to inhibitory cells (Buia & Tiesinga, 2006). Activation of nAChRs has also been reported to increase excitability of neocortical pyramidal cells (Hedrick & Waters, 2015). While this excitability increase may be mediated by changes in intracellular Ca2+ activity, rather than by modulation of membrane K+ currents as occurs with mAChR activation, it would likewise promote gamma rhythmicity by a PING mechanism.

A number of other computational modeling studies have investigated the role of ACh in attention and processing of sensory inputs (Hasselmo *et al.*, 1992; Tiesinga *et al.*, 2001; Borgers *et al.*, 2005; Borgers & Kopell, 2008; Deco & Thiele, 2011; Kanamaru *et al.*, 2013) (see (Newman *et al.*, 2012) for review). In particular, these studies address how ACh modulates network dynamics to support selectivity in network responses to competing external stimuli, or winner-take-all dynamics, as would occur in selective attention tasks (Thiele & Bellgrove, 2018). The contribution of gamma oscillations in selective attention was included in (Borgers & Kopell, 2005; Borgers & Kopell, 2008) where, in the presence of competing external excitatory stimuli, ACh modulation promoted increased gamma activity in the subset of cells receiving stronger stimuli. These studies consider diverse effects of ACh modulation on neuron and network properties including modulation of mAChR-mediated K+ currents (Borgers & Kopell, 2005)and additional K+ and Ca2+ currents (Tiesinga *et al.*, 2001), increases in inhibitory synaptic activity (Borgers & Kopell, 2008), decreases in inhibitory synaptic activity (Kanamaru *et al.*, 2013), or some combination of these effects (Hasselmo *et al.*, 1992; Deco & Thiele, 2011).In related modeling studies of selective attention in visual cortical circuits, attention, simulated as changes in top-down or sensory-associated excitatory drive to E and/or I cells, facilitated selective responses and increased gamma band oscillations and synchrony (Buia & Tiesinga, 2008; Tiesinga & Buia, 2009).

Our results point to a slightly different mechanism for selectivity in processing of competing external stimuli. Namely, spatially localized ACh could bias the network response to be dominated by the activity of the affected excitatory neurons. Their interaction with local

inhibitory neuronscan induce spatially localized gamma which provides the network oscillatory dynamics necessary to promote cognitive processing of stimuli introduced in that local area of the network. Multiple lines of evidence support the contributions of gamma oscillations as important for cognition (Buzsaki & Wang, 2012; Cannon *et al.*, 2014) and integration of sensory input(Singer & Gray, 1995). Thus, we hypothesize, that spatially localized ACh-induced gamma primes the network for successful cognitive processing of spatially coincident stimuli. This provides an additional mechanism or dynamical layer for priming an attentionally activated subnetwork toward integration of sensory information via gamma band oscillations and biasing the network response to be driven by that subpopulation.
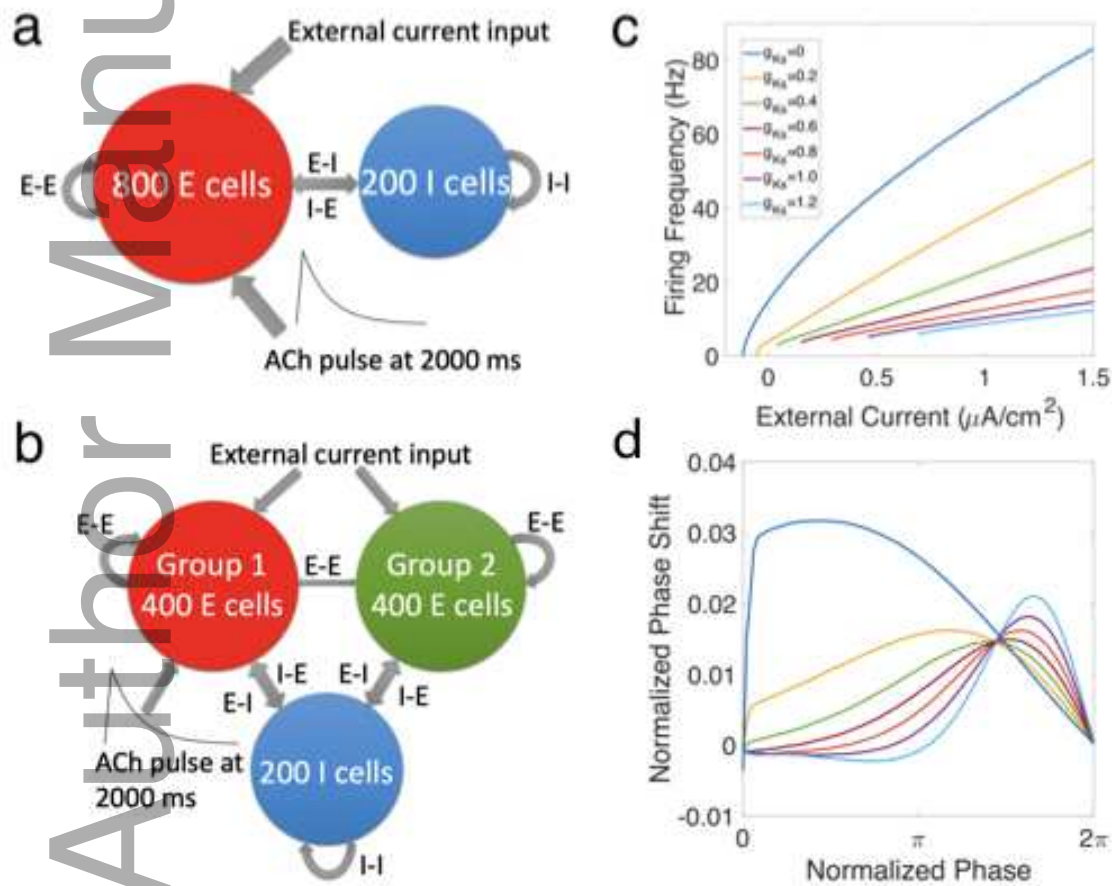
Figure 1: Schematic diagram of network structure and effects of simulated acetylcholine (ACh) modulation on neuronal input-frequency (I-F) curveand phase response curve (PRC).

(a) The network consisted of 800 excitatory cells and 200 inhibitory cells with random connectivity within and between groups. Excitatory cells received external noisy input. AChmodulation was simulated by brief down-regulation of the K^+ M current conductance, g_{Ks}, applied only to excitatory cells (except in results in Figure 6). (b) In a different network configuration for results in Figure 7, excitatory cells are divided into two groups, where only one group (targeted) receives g_{Ks} modulation. (c) Current-frequency (I-F) curves for the Hodgkin-Huxley-type model neuron containing the K^+ M current that is down-regulated by ACh. Different g_{Ks} values correspond to different ACh levels(see Methods). When g_{Ks} is low (high ACh), the neurons are more excitable with higher gain and a Type I profile of the I-F curve. Conversely when $g_{Ks}$is high (low ACh), neuron excitability is lower and I-F curves have Type II profiles.(d) Phase response curves (PRCs) for the model neuron at different g_{Ks} values. When g_{Ks} is low, brief excitatory applied current pulses induce only advances in time of spike firing (positive phase shifts) regardless of their timing (Type I PRC). At high g_{Ks} values, brief excitatory stimuli result in either advances or delays (negative phase shifts) of spike firing depending on their timing (Type II PRC).
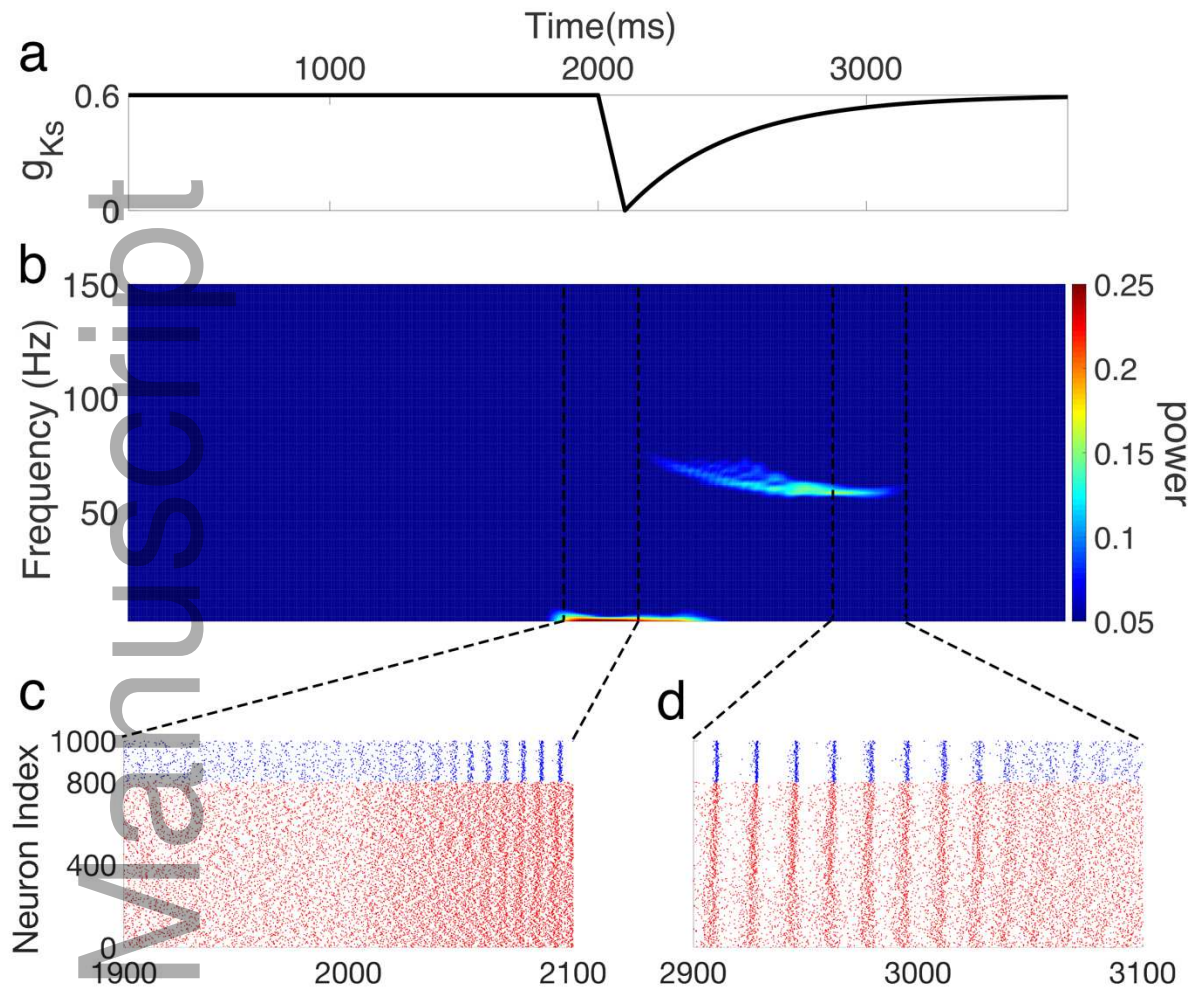
Figure 2: Emergence of gamma oscillations mediated by a simulated AChtransient.
(a) Transient change in maximum conductance of K$^+$ M current,g_{Ks}, simulating AChtransient.
(b)Power spectrogram computed from simulated local field potential (see Methods). Starting at 2000 ms, the g_{Ks}transient led to increasing power in the gamma band. At around 3000 ms, the gamma power dropped back to the default level with the recovery of g_{Ks}. (c) Raster plot showingthe time range at which the network began to change from asynchronousfiring to synchronousgamma oscillations with onset of g_{Ks}transient (excitatory cells in red and inhibitory cells in blue).(d)Raster plot showing the time range during the recovery of the g_{Ks} transient when synchronousgamma oscillations gradually dissipated and the network returned to the asynchronized state.

Before ACh pulse   During ACh pulse   After ACh pulse
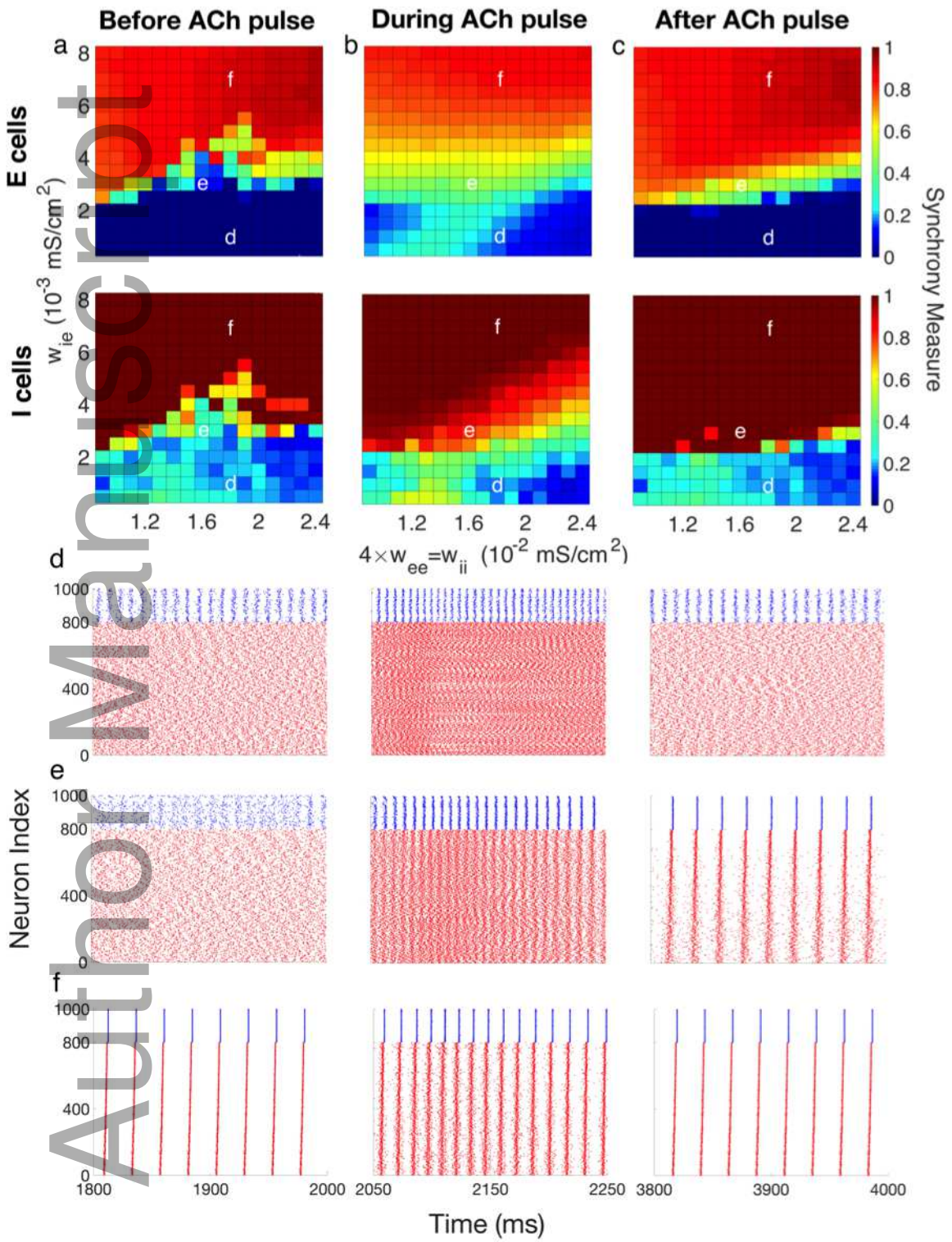
Figure 3: Sensitivity of emergent gamma to network connectivity strength between and among excitatory and inhibitory cells.

(a-c) Synchrony measure (color, see Methods) of excitatory cells (top) and inhibitory cells (bottom) computed in 500 ms time intervals before (left panels), during (middle panels), and after (right panels) the simulated ACh transient, averaged over 5 simulations. Maximum conductances of synaptic currents among the inhibitory cells (I-I synapses, w_{ii}) and among the excitatory cells (E-E synapses, $w_{ee} = 0.25w_{ii}$) are varied on the x-axis and maximum conductances of synaptic currents from the inhibitory cells to the excitatory cells (I-E synapses, w_{ie}) is varied on the y-axis (conductance of E-I synapses was fixed at $w_{ei} = 0.002$ mS/cm^2). (a) Before the g_{Ks}transient (1500-2000 ms), networks exhibited synchronous or asynchronous firing depending on the connectivity strengths. (b) During the g_{Ks}transient (2050-2550 ms), synchronousgamma oscillations were exhibited by networks in a wider range of connectivity strengths.(c) After the g_{Ks} transientrecovered (3500-4000 ms), gamma oscillations were maintained in networksin some synaptic strength parameter regimes (compare with (a)), or network activity returned to the pre-stimulus state. (d-f) Raster plots showing network firing for synaptic strength values indicated in (a-c) during time intervals before (left), during (middle) and after (right) the g_{Ks}transient (excitatory cells in red, inhibitory cells in blue). The parameter values used in (e) are the same as in Figure 2. External random noise was not included in these simulations.
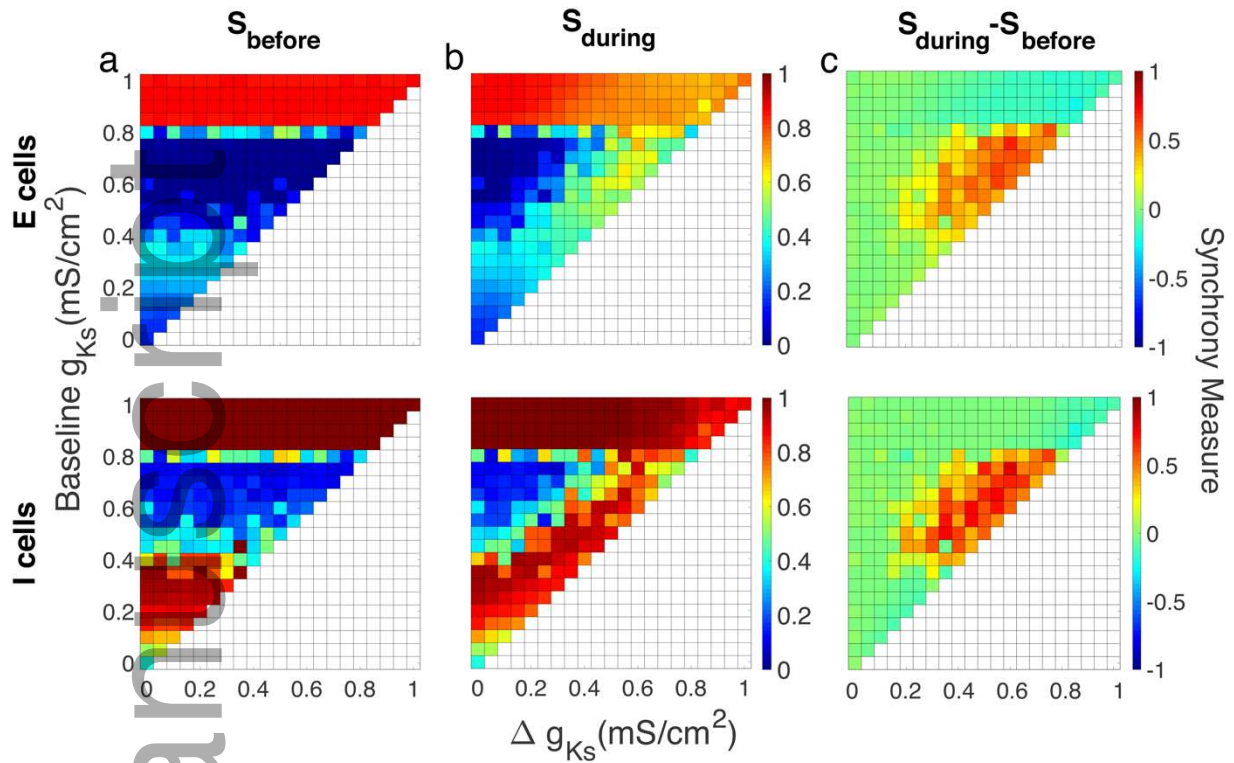
Figure 4: Sensitivity of emergent gamma on magnitude of simulated ACh effects. Magnitudes of the maximum conductance of the K^+ M current before and after the simulated ACh transient, baseline $\overline{g_{Ks}}$ (y-axes), andof the maximum change in g_{Ks} during the ACh transient, Δg_{Ks} (x-axes), were varied. Synchrony measures (color) for excitatory cells (top) and inhibitory cells (bottom) computed in 500 ms time intervals before the ACh transient (a) and during the ACh transient (b).(c) Differences in synchrony measures computed before and during the transient highlight parameter regimes in which gamma synchrony is most affected. Gamma synchrony was reliably induced for moderate values of both baseline $\overline{g_{Ks}}$ and Δg_{Ks} (from around 0.4 mS/cm^2 to 0.8 mS/cm^2).
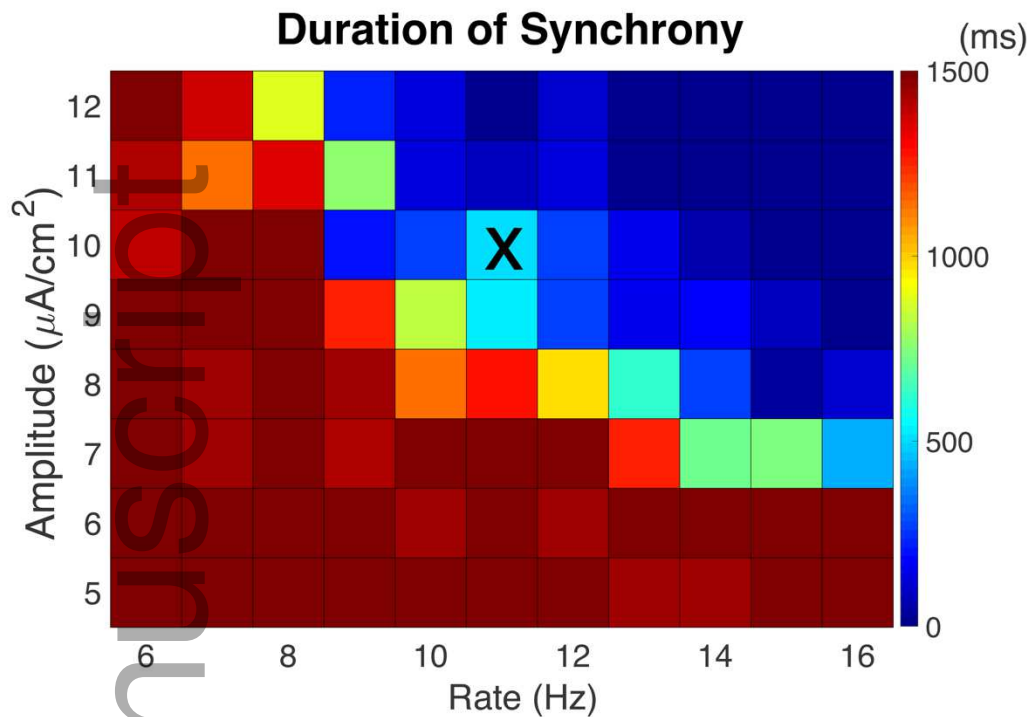
Figure 5: Duration of gamma synchrony in the presence of external random noise. External noise can drive the synchronized network back to asynchrony as the g_{Ks} transient recovers. Color shows the average time duration (in ms) of gamma synchronyinduced by the g_{Ks}transient for different amplitudes(y-axis) and rates(x-axis) of brief, depolarizing kick stimuli delivered as arandom Poisson process to each neuron. When the amplitude and rate were small, synchronous gamma remained stable (duration >1500 ms) after the g_{Ks} transientrecovered. When the amplitude and/or rate were large, the noise prohibited the network from displaying gamma synchrony even during the g_{Ks} pulse. Results are averaged over 5 simulation runs. Noise parameters for simulations displayed in Figure 2 are indicated by 'X'.
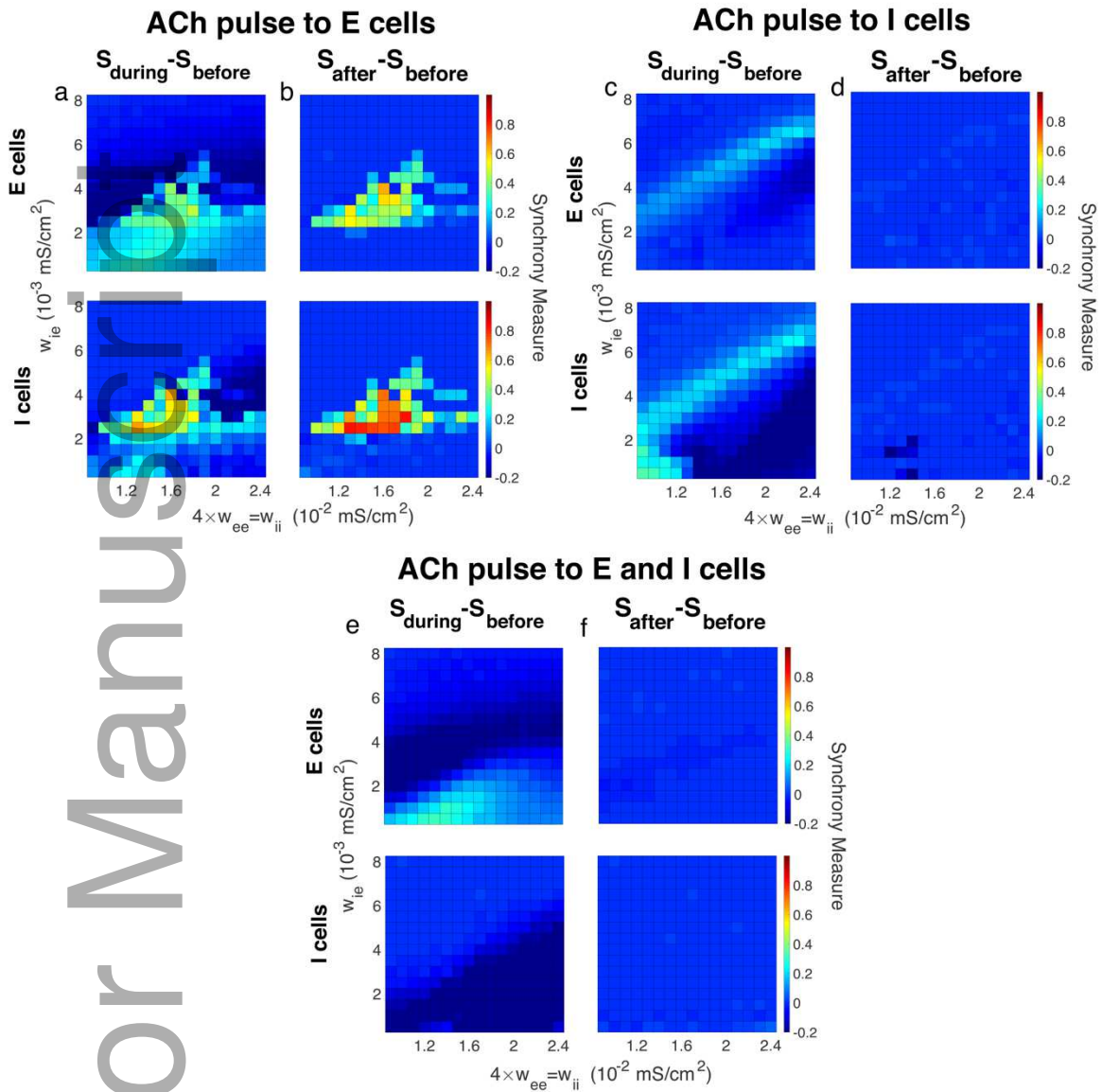
Figure 6: Induction of gamma synchrony by simulated AChmodulation to only inhibitory cells or to both excitatory and inhibitory cells. Differences in synchrony measures (color) between before and during (a, c, e) the g_{Ks} transient, and between before and after (b, d, f) the g_{Ks} transient for excitatory cells (top panels) and inhibitory cells (bottom panels) whenthe transient was applied to only excitatory cells (a, b), to only inhibitory cells (c, d), or to both excitatory and inhibitory cells (e, f). Panel (a) [(b)] is the difference between Figure 3 panels (b) and (a) [(c) and (a)].Simulated ACh modulation to only inhibitory cells or to both excitatory and inhibitory cells did not effectively induce gamma synchrony and network activity returned to its initial state after the g_{Ks} transient recovered. External random noise was not included in these simulations.

a

Group 2
nontargeted

Group 1
targeted

Fourier transform (Group 1)

b

power

Fourier transform (Group 2)

c

power

d

Group1
Group2
Inhibitory cells

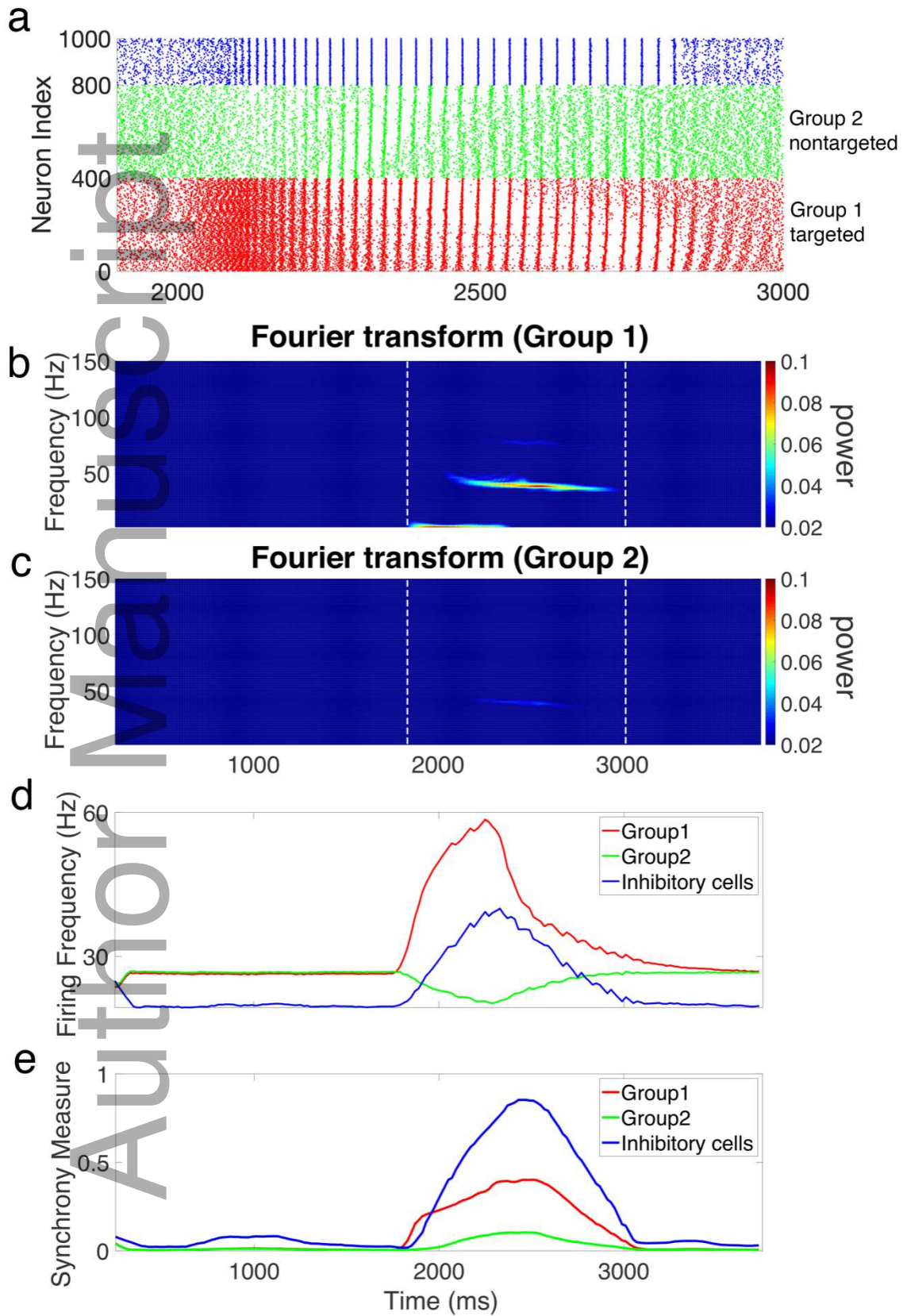**e**

Group1
Group2
Inhibitory cells

Figure 7: Spatially localized simulated ACh modulation generates local gamma.

(a) Raster plot from the network structure illustrated in Figure 1b when the g_{Ks} transient is only applied to group 1 excitatory cells (red, index:1-400). During the transient, the activity of group 2 excitatory cells (green, index: 410-800) is slightly inhibited, while the group 1 excitatory cells (red) and inhibitory cells (blue, index: 801-1000) show higher activity and synchronization. (b-c) Power spectrogram of the simulated local field potential of group 1 excitatory cells and group 2 excitatory cells, respectively. The power of gamma oscillation for group 1 cells is stronger than group 2 cells during the g_{Ks} transient. Change of average firing frequency over time ((c), see Methods) and change of synchrony measure over time ((d), see Methods) showed that the targeted excitatory cells (group 1, red) and inhibitory cells (blue) increased their firing and synchrony during g_{Ks} modulation while non-targeted excitatory cells (green) showed decreased firing and only very weak synchrony during the g_{Ks} transient.

References

Ascoli, G.A. & Atkeson, J.C. (2005) Incorporating anatomically realistic cellular-level connectivity in neural network models of the rat hippocampus. *Biosystems*, **79**, 173-181.

Bogaard, A., Parent, J., Zochowski, M. & Booth, V. (2009) Interaction of cellular and network mechanisms in spatiotemporal pattern formation in neuronal networks. *J Neurosci*, **29**, 1677-1687.

Borgers, C., Epstein, S. & Kopell, N.J. (2005) Background gamma rhythmicity and attention in cortical local circuits: a computational study. *Proc Natl Acad Sci U S A*, **102**, 7002-7007.

Borgers, C. & Kopell, N. (2005) Effects of noisy drive on rhythms in networks of excitatory and inhibitory neurons. *Neural Comput*, **17**, 557-608.

Borgers, C. & Kopell, N.J. (2008) Gamma oscillations and stimulus selection. *Neural Comput*, **20**, 383-414.

Buia, C. & Tiesinga, P. (2006) Attentional modulation of firing rate and synchrony in a model cortical network. *J Comput Neurosci*, **20**, 247-264.

Buia, C.I. & Tiesinga, P.H. (2008) Role of interneuron diversity in the cortical microcircuit for attention. *J Neurophysiol*, **99**, 2158-2182.

Buzsaki, G. & Wang, X.J. (2012) Mechanisms of gamma oscillations. *Annu Rev Neurosci*, **35**, 203-225.

Cannon, J., McCarthy, M.M., Lee, S., Lee, J., Borgers, C., Whittington, M.A. & Kopell, N. (2014) Neurosystems: brain rhythms and cognitive processing. *Eur J Neurosci*, **39**, 705-719.

Colangelo, C., Shichkova, P., Keller, D., Markram, H. & Ramaswamy, S. (2019) Cellular, Synaptic and Network Effects of Acetylcholine in the Neocortex. *Front Neural Circuits*, **13**, 24.

Couey, J.J., Meredith, R.M., Spijker, S., Poorthuis, R.B., Smit, A.B., Brussaard, A.B. & Mansvelder, H.D. (2007) Distributed network actions by nicotine increase the threshold for spike-timing-dependent plasticity in prefrontal cortex. *Neuron*, **54**, 73-87.

Deco, G. & Thiele, A. (2011) Cholinergic control of cortical network interactions enables feedback-mediated attentional modulation. *Eur J Neurosci*, **34**, 146-157.

Disney, A.A. & Aoki, C. (2008) Muscarinic acetylcholine receptors in macaque V1 are most frequently expressed by parvalbumin-immunoreactive neurons. *J Comp Neurol*, **507**, 1748-1762.

Ermentrout, B. (1996) Type I membranes, phase resetting curves, and synchrony. *Neural Comput*, **8**, 979-1001.

Fink, C.G., Booth, V. & Zochowski, M. (2011) Cellularly-driven differences in network synchronization propensity are differentially modulated by firing frequency. *PLoS Comput Biol*, **7**, e1002062.

Gielow, M.R. & Zaborszky, L. (2017) The input-output relationship of the cholinergic basal forebrain. *Cell Reports*, **18**, 1817-1830.

Golomb, D. & Rinzel, J. (1993) Dynamics of globally coupled inhibitory neurons with heterogeneity. *Phys Rev E Stat Phys Plasmas Fluids Relat Interdiscip Topics*, **48**, 4810-4814.

Golomb, D. & Rinzel, J. (1994) Clustering in Globally Coupled Inhibitory Neurons. *Physica D*, **72**, 259-282.

Gritton, H.J., Howe, W.M., Mallory, C.S., Hetrick, V.L., Berke, J.D. & Sarter, M. (2016) Cortical cholinergic signaling controls the detection of cues. *Proc Natl Acad Sci U S A*, **113**, E1089-1097.

Hasselmo, M.E., Anderson, B.P. & Bower, J.M. (1992) Cholinergic modulation of cortical associative memory function. *J Neurophysiol*, **67**, 1230-1246.

Hedrick, T. & Waters, J. (2015) Acetylcholine excites neocortical pyramidal neurons via nicotinic receptors. *J Neurophysiol*, **113**, 2195-2209.

Howe, W.M., Berry, A.S., Francois, J., Gilmour, G., Carp, J.M., Tricklebank, M., Lustig, C. & Sarter, M. (2013) Prefrontal cholinergic mechanisms instigating shifts from monitoring for cues to cue-guided performance: converging electrochemical and fMRI evidence from rats and humans. *J Neurosci*, **33**, 8742-8752.

Howe, W.M., Gritton, H.J., Lusk, N.A., Roberts, E.A., Hetrick, V.L., Berke, J.D. & Sarter, M. (2017) Acetylcholine Release in Prefrontal Cortex Promotes Gamma Oscillations and Theta-Gamma Coupling during Cue Detection. *J Neurosci*, **37**, 3215-3230.

Kanamaru, T., Fujii, H. & Aihara, K. (2013) Deformation of attractor landscape via cholinergic presynaptic modulations: a computational study using a phase neuron model. *PLoS One*, **8**, e53854.

Kim, K., Muller, M., Bohnen, N.I., Sarter, M. & Lustig, C. (2017) The cortical cholinergic system contributes to the top-down control of distraction: Evidence from patients with Parkinson's disease. *Neuroimage*, in press.

Krnjevic, K. (2004) Synaptic mechanisms modulated by acetylcholine in cerebral cortex. *Prog Brain Res*, **145**, 81-93.

McCormick, D.A. & Prince, D.A. (1985) Two types of muscarinic response to acetylcholine in mammalian cortical neurons. *Proc Natl Acad Sci U S A*, **82**, 6344-6348.

McGaughy, J., Kaiser, T. & Sarter, M. (1996) Behavioral vigilance following infusions of 192 IgG-saporin into the basal forebrain: selectivity of the behavioral impairment and relation to cortical AChE-positive fiber density. *Behav Neurosci*, **110**, 247-265.

Newman, E.L., Gupta, K., Climer, J.R., Monaghan, C.K. & Hasselmo, M.E. (2012) Cholinergic modulation of cognitive processing: insights drawn from computational models. *Front Behav Neurosci*, **6**, 24.

Obermayer, J., Heistek, T.S., Kerkhofs, A., Goriounova, N.A., Kroon, T., Baayen, J.C., Idema, S., Testa-Silva, G., Couey, J.J. & Mansvelder, H.D. (2018) Lateral inhibition by Martinotti interneurons is facilitated by cholinergic inputs in human and mouse neocortex. *Nat Commun*, **9**, 4101.

Parikh, V., Kozak, R., Martinez, V. & Sarter, M. (2007) Prefrontal acetylcholine release controls cue detection on multiple timescales. *Neuron*, **56**, 141-154.

Sarter , M. & Lustig, C. (2019) Forebrain Cholinergic Signaling: Wired and Phasic, not Tonic, and Causing Behavior. *Preprints*, **2019040010** 2019040010

Sarter, M. & Lustig, C. (2019) Forebrain cholinergic signaling: Wired and phasic, not tonic, and causing behavior. *J Neurosci (in press)*.

Singer, W. & Gray, C.M. (1995) Visual feature integration and the temporal correlation hypothesis. *Annu Rev Neurosci*, **18**, 555-586.

Stiefel, K.M., Gutkin, B.S. & Sejnowski, T.J. (2008) Cholinergic neuromodulation changes phase response curve shape and type in cortical pyramidal neurons. *PLoS One*, **3**, e3947.

Stiefel, K.M., Gutkin, B.S. & Sejnowski, T.J. (2009) The effects of cholinergic neuromodulation on neuronal phase-response curves of modeled cortical neurons. *J Comput Neurosci*, **26**, 289-301.

Thiele, A. & Bellgrove, M.A. (2018) Neuromodulation of Attention. *Neuron*, **97**, 769-785.

Tiesinga, P. & Sejnowski, T.J. (2009) Cortical enlightenment: are attentional gamma oscillations driven by ING or PING? *Neuron*, **63**, 727-732.

Tiesinga, P.H. & Buia, C.I. (2009) Spatial attention in area V4 is mediated by circuits in primary visual cortex. *Neural Netw*, **22**, 1039-1054.

Tiesinga, P.H., Fellous, J.M., Jose, J.V. & Sejnowski, T.J. (2001) Computational model of carbachol-induced delta, theta, and gamma oscillations in the hippocampus. *Hippocampus*, **11**, 251-274.

Urban-Ciecko, J., Jouhanneau, J.S., Myal, S.E., Poulet, J.F.A. & Barth, A.L. (2018) Precisely Timed Nicotinic Activation Drives SST Inhibition in Neocortical Circuits. *Neuron*, **97**, 611-625 e615.

Viriyopase, A., Memmesheimer, R.M. & Gielen, S. (2016) Cooperation and competition of gamma oscillation mechanisms. *J Neurophysiol*, **116**, 232-251.
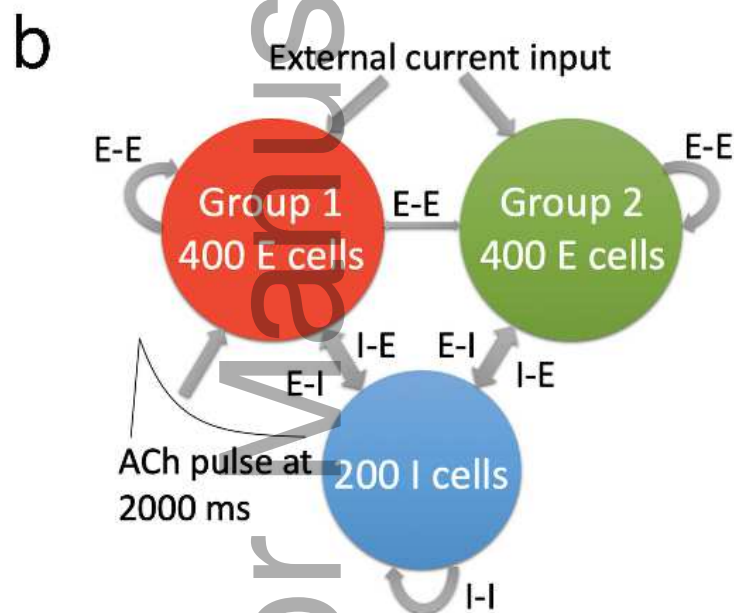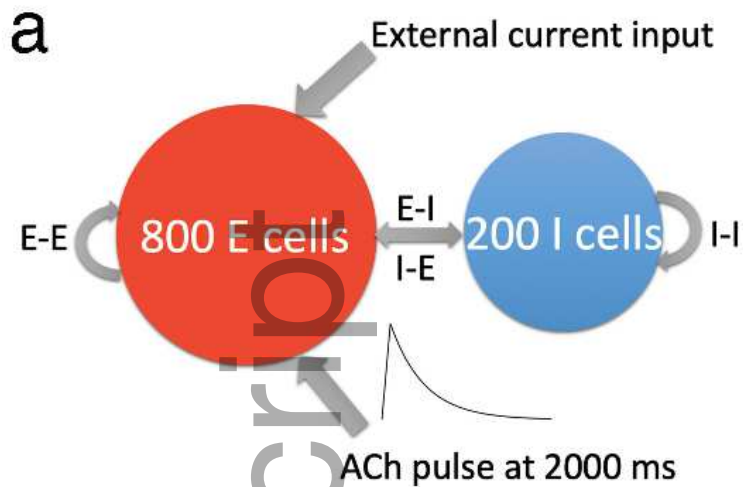
Whittington, M.A., Traub, R.D., Kopell, N., Ermentrout, B. & Buhl, E.H. (2000) Inhibition-based rhythms: experimental and mathematical observations on network dynamics. *Int J Psychophysiol*, **38**, 315-336.

Yuan, R., Biswal, B.B. & Zaborszky, L. (2018) Functional Subdivisions of Magnocellular Cell Groups in Human Basal Forebrain: Test-Retest Resting-State Study at Ultra-high Field, and Meta-analysis. *Cereb Cortex*.
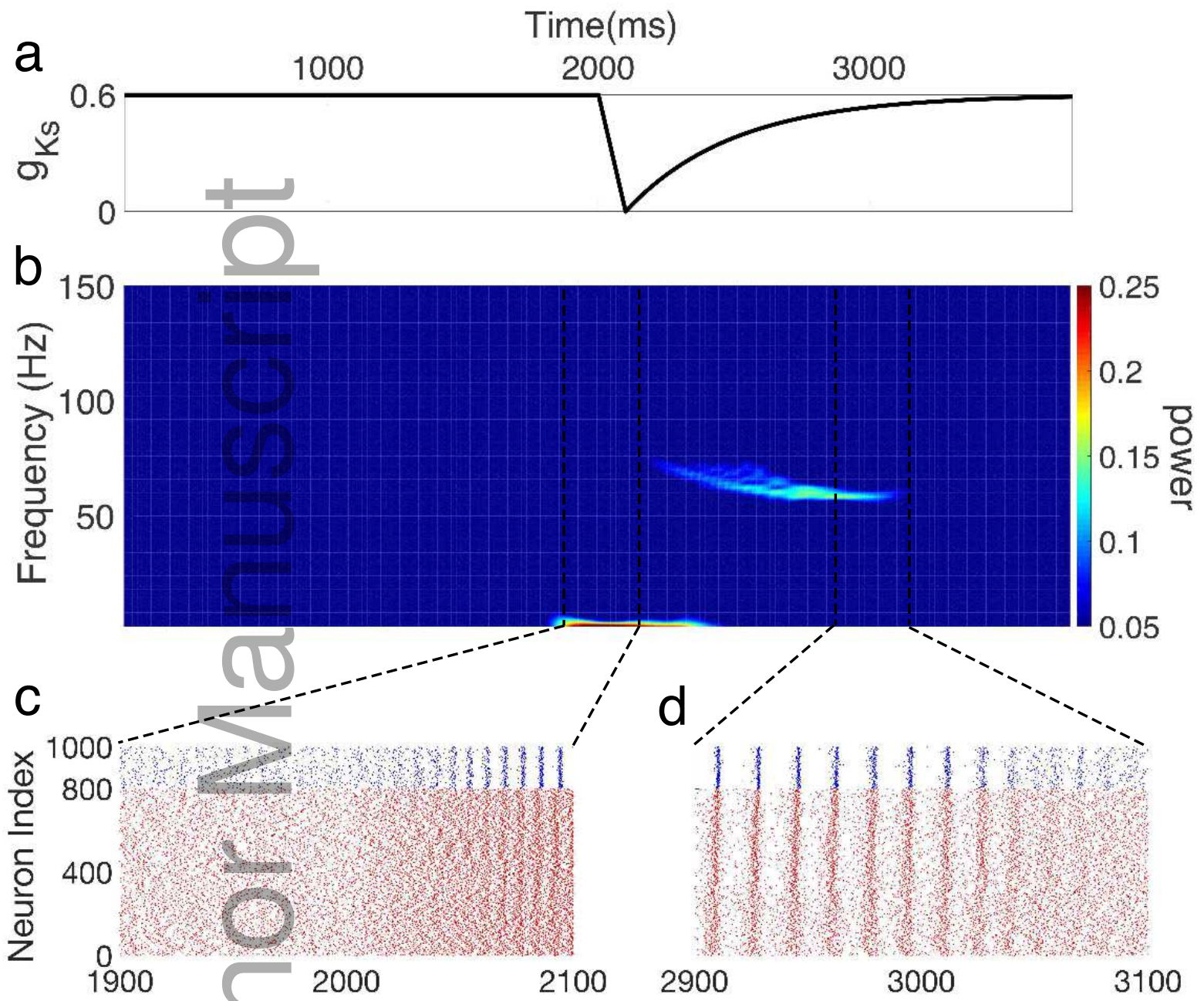
Zaborszky, L., Buhl, D.L., Pobalashingham, S., Bjaalie, J.G. & Nadasdy, Z. (2005) Three-

dimensional chemoarchitecture of the basal forebrain: spatially specific association of

cholinergic and calcium binding protein-containing neurons. *Neuroscience*, **136**, 697-713.

Zaborszky, L., Duque, A., Gielow, M., Gombkoto, P., Nadasdy, Z. & Somogyi, J. (2015)

Organization of the basal forebrain cholinergic projection system: Specific or diffuse? In

Paxinos, G. (ed) *The rat nervous system*. Academic Press, San Diego, pp. 491-507.
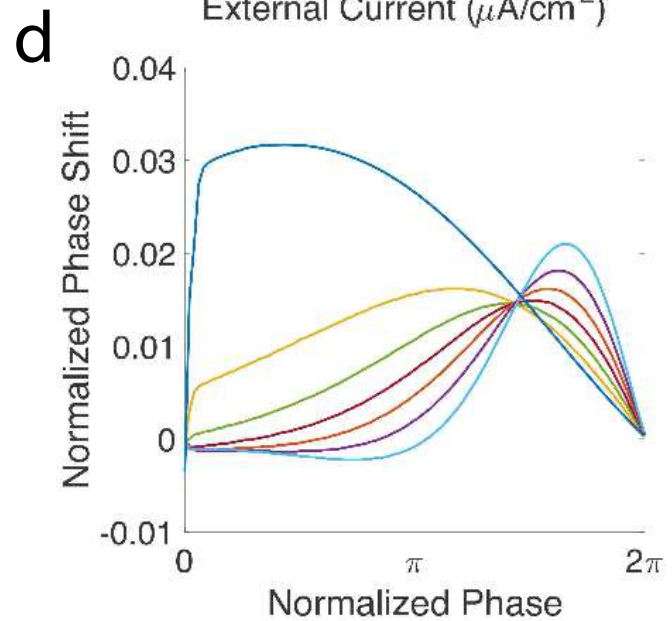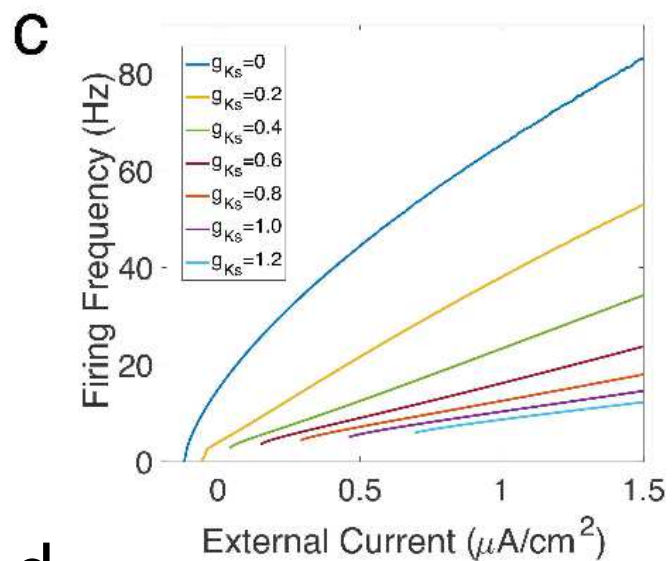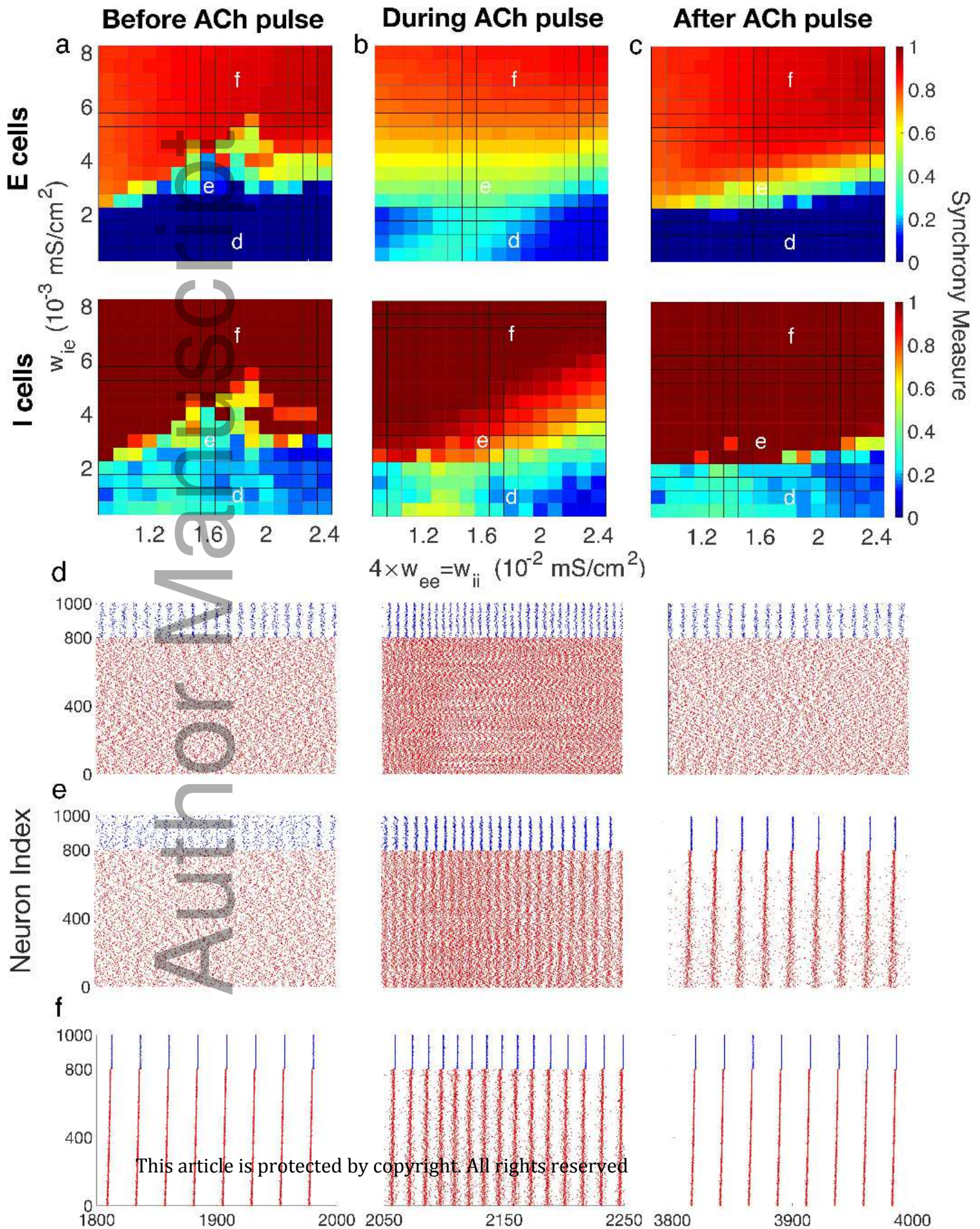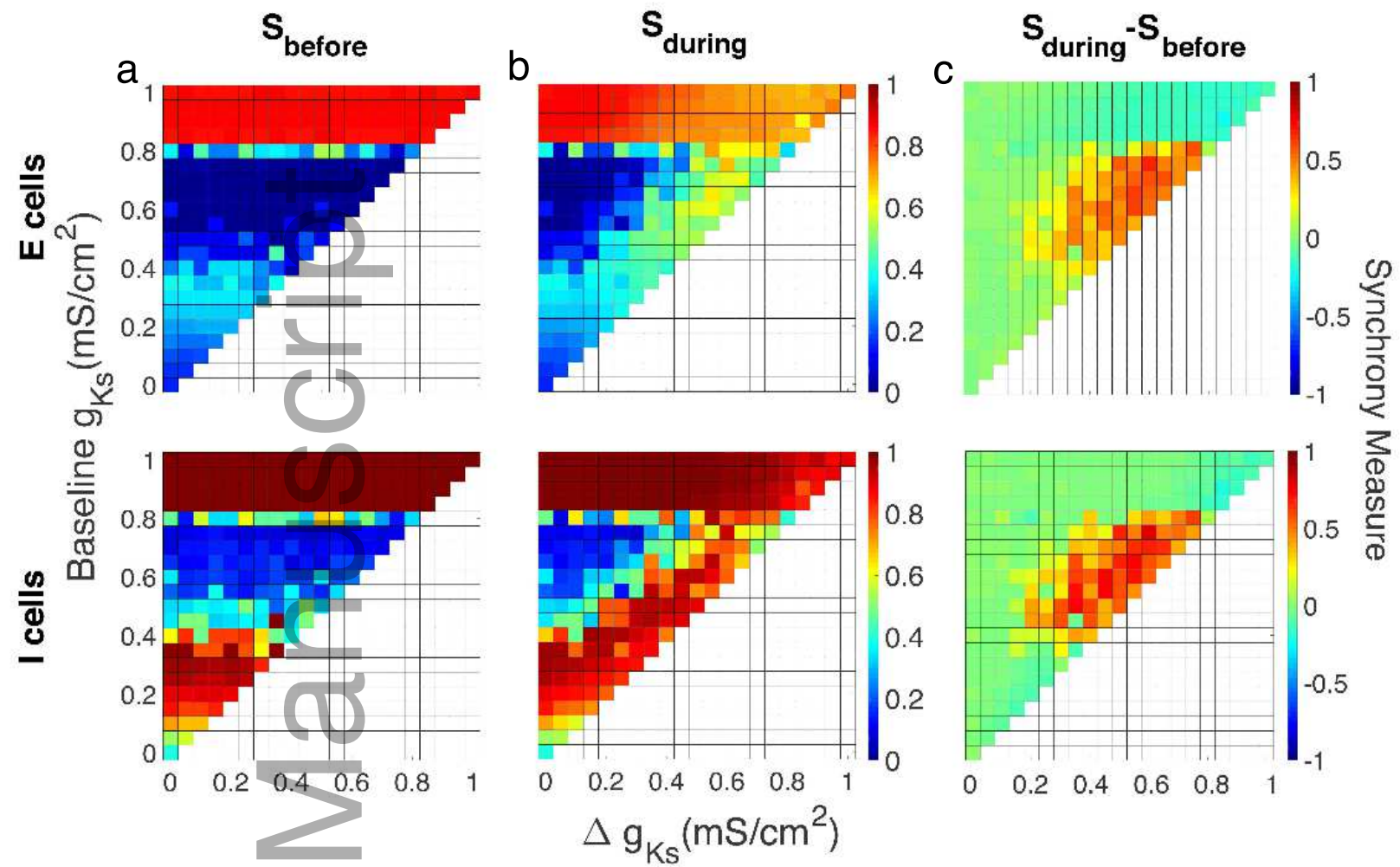
ejn_14744_f1.eps

ejn_14744_f2.eps
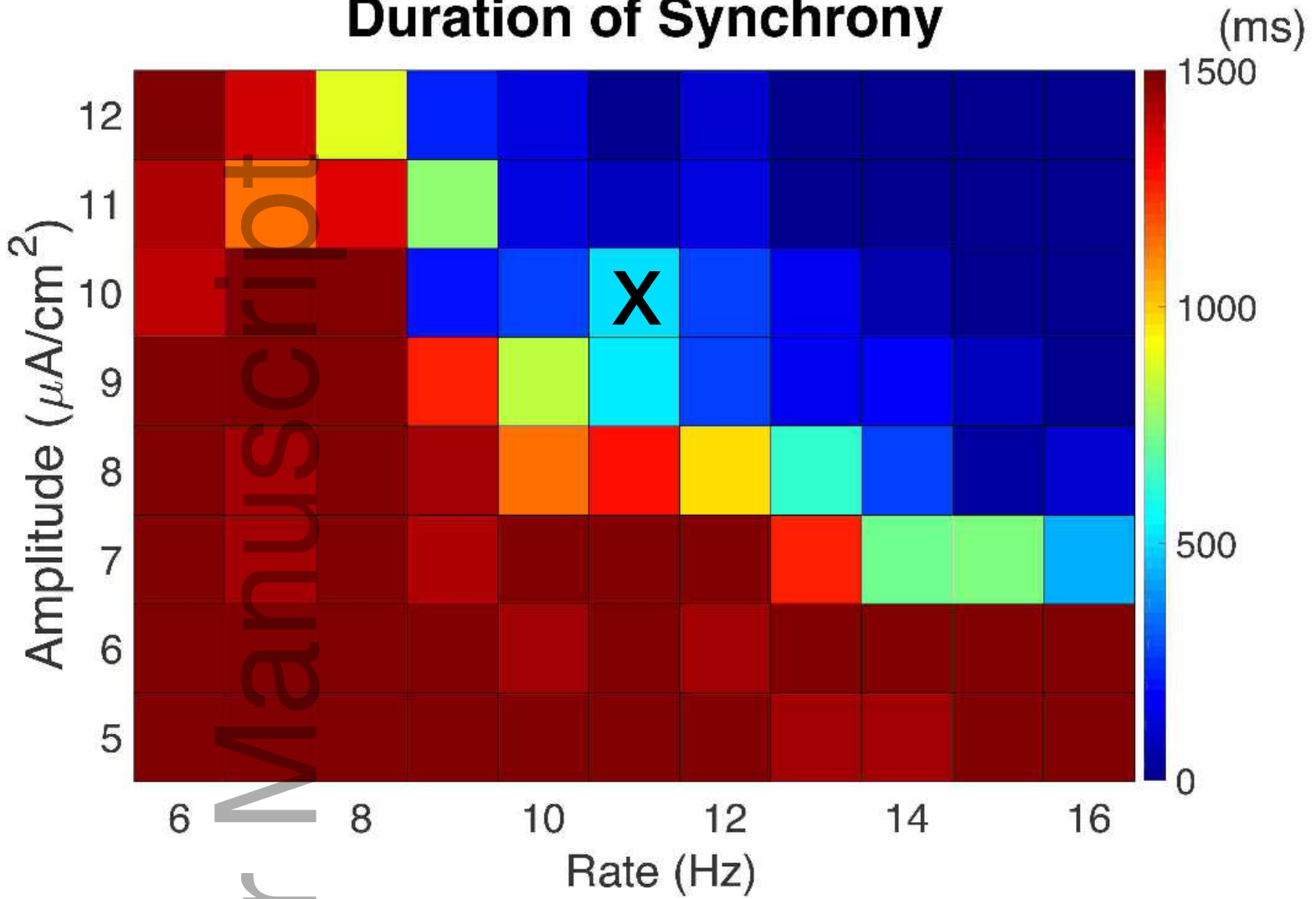
Before ACh pulse   **During ACh pulse**   **After ACh pulse**

a   b   c

E cells

w_{ie} (10^{-3} mS/cm^2)

Synchrony Measure

I cells

$4 \times w_{ee} = w_{ii}$ (10^{-2} mS/cm^2)

d

e

Neuron Index

f

S_before   S_during   S_during-S_before

ejn_14744_f4.eps

Duration of Synchrony

ejn_14744_f5.eps

ACh pulse to E cells

a $S_{during} - S_{before}$ b $S_{after} - S_{before}$

ACh pulse to I cells

c $S_{during} - S_{before}$ d $S_{after} - S_{before}$
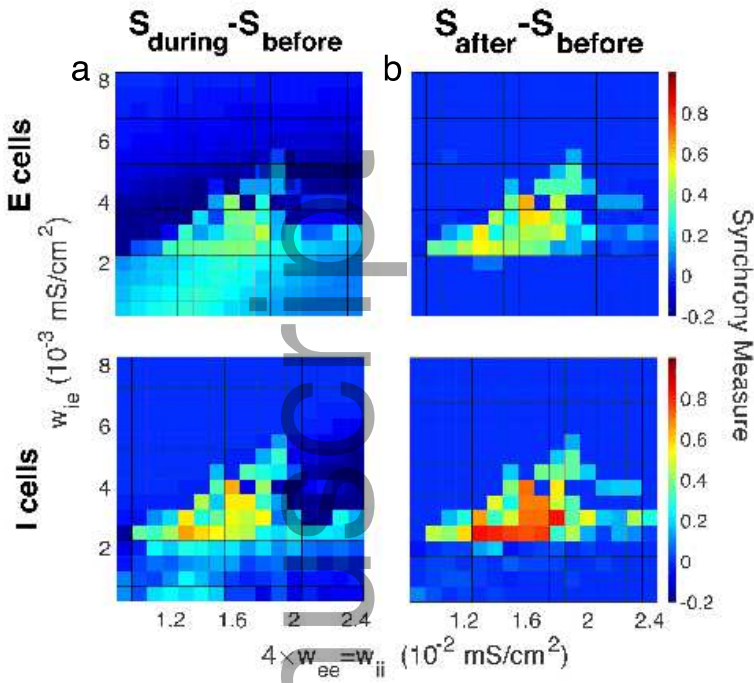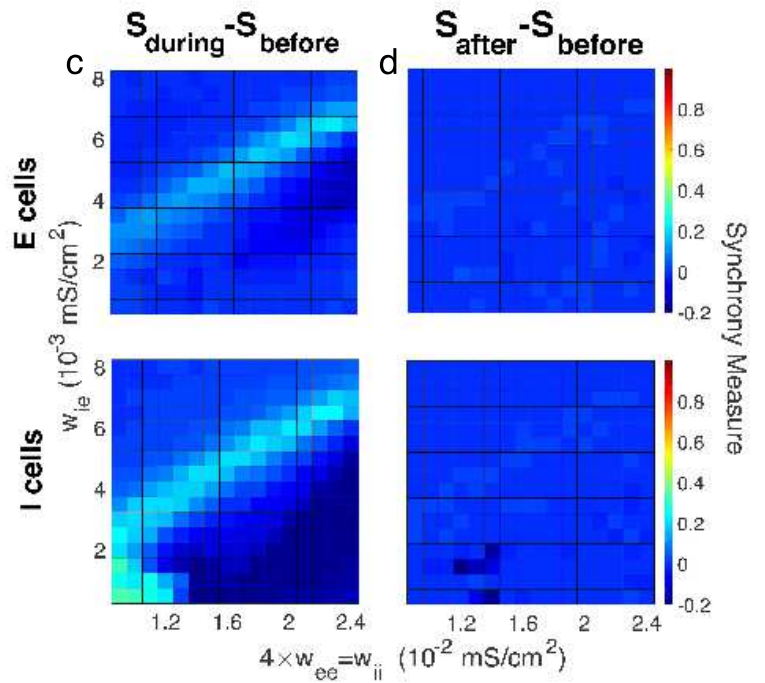
ACh pulse to E and I cells

e $S_{during} - S_{before}$ f $S_{after} - S_{before}$

w_{ie} (10^{-3} mS/cm^2)

$4 \times w_{ee} = w_{ii}$ (10^{-2} mS/cm^2)

Synchrony Measure

ejn_14744_f6.eps

a

Group 2
nontargeted

Group 1
targeted

Fourier transform (Group 1)

power

Fourier transform (Group 2)

power

d

e